# Orchestrating spontaneous emission with metasurfaces: recent advances in engineering thermal, luminescent and quantum emissions

*Hyosim Yang Wesley Mills Sathwik Bharadwaj Saaketh Desai Tomás Santiago-Cruz Samuel Prescott Oleg Mitrofanov Igal Brener Jon Schuller Zubin Jacob Prasad P Iyer**

Wesley Mills, Jon Schuller
Address: University of California, Santa Barbara, California, USA

Samuel Prescott, Oleg Mitrofanov
University College London,London WC1E 6BT, United Kingdom

Sathwik Bharadwaj, Zubin Jacob
Purdue University, West Lafayette, Indiana, USA

Hyosim Yang, Tomás Santiago-Cruz, Saaketh Desai, Igal Brener, Prasad Iyer
Center for Integrated Nanotechnologies, Sandia National Lab, Albuquerque, New Mexico, USA
Email Address: *ppadma@sandia.gov

Keywords: *Metasurfaces, Thermal emission, Quantum Emission, Luminescence*

Metasurfaces have emerged as powerful tools for controlling spontaneous emission, offering unprecedented control over light-matter interactions at sub-wavelength scales. While metasurfaces have been traditionally utilized for shaping coherent electromagnetic waves, they have recently extended their capabilities to control incoherent or spontaneous emission. We review how metasurfaces can enhance and precisely control properties of thermal, luminescent, and quantum emission. In thermal emission, metasurfaces enable control over spatial, temporal, and spin coherence, offering new possibilities for applications such as energy harvesting, radiative cooling and heat assisted ranging and detection. For luminescent emission, metasurfaces significantly improve emission rates, quantum efficiency, and directionality, driving innovations in lighting and display technologies. For controlling quantized spontaneous emission, metasurfaces have been instrumental in enhancing single-photon sources and enabling novel functionalities in quantum states through photon-pair generation, which is vital for quantum communication, meteorology, and computing. Despite these advancements several challenges to increase the operational bandwidths, accelerate and develop simulation strategies, and fabrication complexities persist. We also discuss emerging trends, such as dynamic metasurfaces and their integration with nanophotonic platforms, which could further expand the capabilities of light-emitting metasurfaces.



## Introduction

Metasurfaces structure light-matter interactions at the sub-wavelength scale, enabling novel light functionalities beyond conventional bulky optical components. Metasurfaces, consisting of sub-wavelength arrays of optical resonators, exert nearly complete control over the phase, amplitude, and polarization of light, which allows arbitrary transformations by manipulating the spatial properties of the electromagnetic wavefront. These optical resonators are primarily designed as sub-wavelength scatterers of light, with refractive index and geometry enhance light-matter interactions, especially for coherent light sources. Specifically, holographic transformations of coherent electromagnetic wavefronts can be achieved through judicious engineering of spatial-phase relationships among optical resonators across the metasurface. Consequently, metasurface designs have traditionally focused on manipulating coherent light sources, reinforcing the notion that metasurfaces may not be suitable for controlling spontaneous emission or incoherent light sources.

Spontaneous emission, a fundamental quantum mechanical phenomenon, occurs when an excited electron in an atom or molecule transitions to its ground state, emitting a photon. This process underpins various optical technologies, enabling a range of optoelectronic devices (including incandescent bulbs, thermal lamps, LEDs, etc.), which are ubiquitously used in energy-efficient displays, illumination, optical communications, and sensing systems. With the emergence of single and entangled photons (generated via spontaneous emission) as promising qubit candidates for quantum information systems, the applications

This is the author manuscript accepted for publication and has undergone full peer review but has not been through the copyediting, typesetting, pagination and proofreading process, which may lead to differences between this version and the Version of Record. Please cite this article as doi: 10.1002/adom.202402755

utilizing spontaneous emission continues to grow. However, lack of control over the emitted photon's phase, direction, and temporal coherence, as well as the inherent randomness, limits the performance and efficiency of devices relying on spontaneous emission. Given the nature of spontaneous emission, improving emission (or detection) efficiency while controlling the incoherent electromagnetic wavefront remains a longstanding challenge. Recent developments in phased-array metasurfaces have challenged these limitations, demonstrating that metasurfaces can indeed control spontaneous emission to enhance emission, realize wavefront control, and detect far-field incoherent emissions. Metasurfaces open new pathways for controlling spontaneous emission through nanoscale engineering of light-matter interactions, offering potential solutions to longstanding challenges in the field of light-emitting devices and sensing systems.

Researchers have used plasmonic metasurfaces to enhance the emission rates of quantum emitters, achieving a high degree of directionality and polarization control [1]. Metasurfaces have also been employed to modify the local density of optical states (LDOS) [2, 3], thereby altering the emission properties of embedded emitters. These pioneering efforts demonstrate the possibility of engineering the spontaneous emission process, leading to more efficient and tunable light sources. However, despite these initial successes, several challenges remain. Many of these studies have been limited by issues such as narrow spectral bandwidth, complex fabrication processes, and the difficulty in completely controlling all aspects of the emission process, including temporal and spatial coherence. Addressing these challenges is crucial for advancing the field and for realizing the full potential of metasurfaces in controlling spontaneous emission.

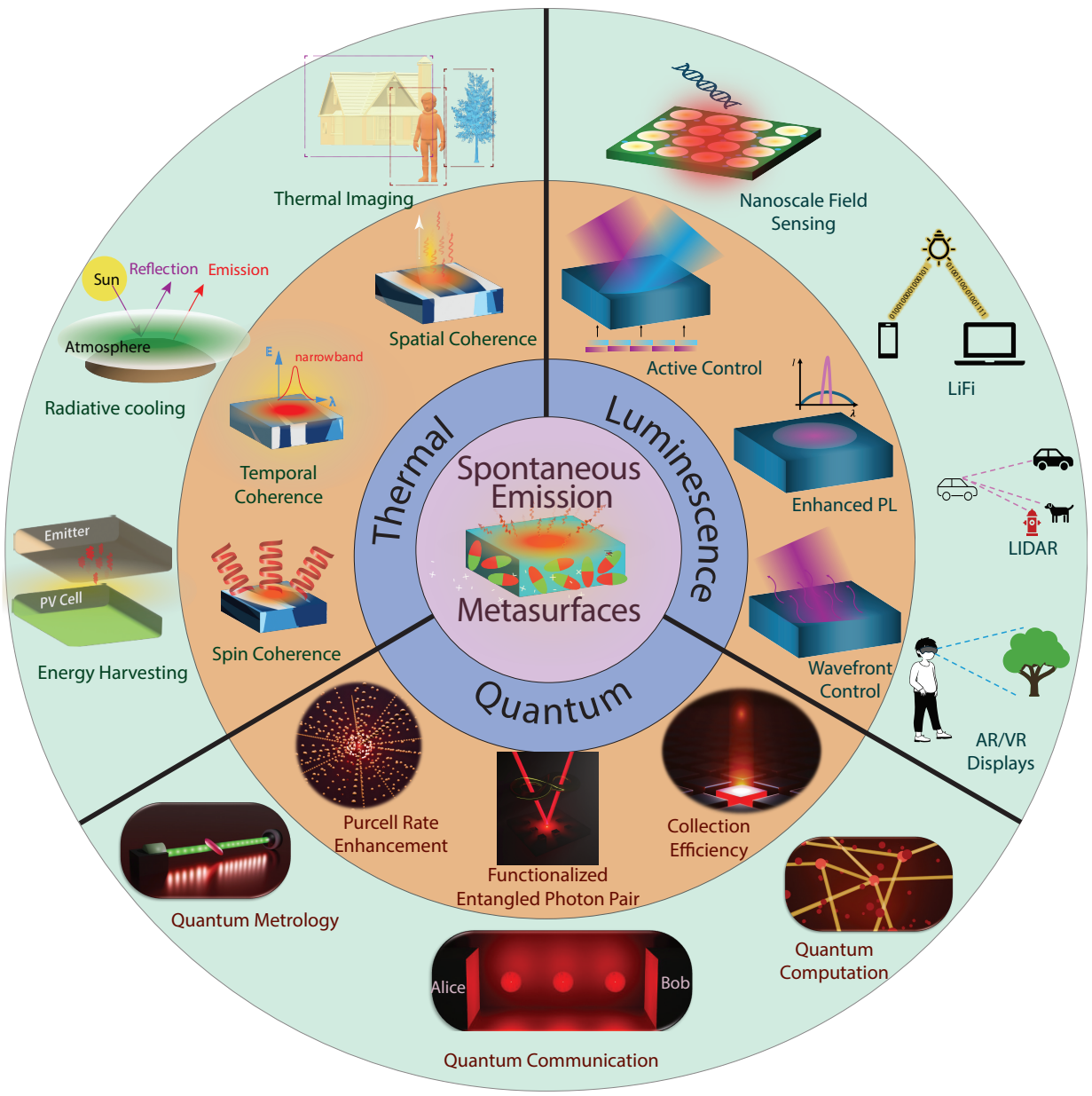


Figure 1: Overview of the review highlighting the novel functionalities (orange circle) realized using metasurfaces and their applications (green circle).

Here, we provide an overview of the progress made in controlling spontaneous emission using metasurfaces (see Fig. 1). We categorize spontaneous emission into three major types: thermal, luminescent, and quantum, each presenting unique challenges and opportunities for control. For thermal emission, we discuss approaches for achieving spatial, temporal, and spin coherence using metasurfaces. We also highlight unique applications enabled by metasurfaces for sensing far-field thermal emissions. In the case of luminescent devices—i.e., arrays or clusters of incoherent emitters—we explore strategies to improve emission efficiency and directivity, as well as to achieve active control of emission by embedding the emitters in the metasurface. Finally, for quantum emission, we examine recent advances in on-demand single-photon sources and the control of photon-pair generation using metasurfaces. We review the current state of the art in this field and identify key challenges that must be addressed to fully realize the potential of metasurfaces in controlling spontaneous emission. Additionally, we discuss future directions and emerging trends, such as the integration of metasurfaces into other nanophotonic platforms and the development of active metasurfaces capable of dynamically controlling emission properties.

## Background

Spontaneous emission is a fundamental process where an excited state decays into a ground state without an external influence, while releasing a photon. While spontaneous emission is often considered an inherently random process with finite uncertainties, metasurfaces have emerged as powerful tools for manipulating its spectral, spatial, and temporal coherence properties. Here, we categorize spontaneous emission into three primary types: thermal emission, photoluminescence (PL), and spontaneous parametric down-conversion (SPDC), while describing the underlying principles and the role of metasurfaces in controlling these processes.

**a. Thermal Emission**: The temperature and emissivity of a black body are inextricably linked to its thermal emission. A blackbody produces omnidirectional and unpolarized electromagnetic fields across a wide wavelength range. By adjusting the temperature or emissivity of the systems one can engineer the properties of thermal emission. Theoretically, the thermal emitters can be characterized by their angular spectrum absorptivity $\alpha(\lambda, \hat{n}, \mathbf{p})$ and emissivity $\eta(\lambda, \hat{n}, \mathbf{p})$, where $\lambda$ is the wavelength, $\hat{n}$ represents the directional vector, and $\mathbf{p}$ is the polarization. The emissivity $\eta(\lambda, \hat{n}, \mathbf{p})$ is given by

$$\eta(\lambda, \hat{n}, \mathbf{p}) = \frac{I(\lambda, \hat{n}, \mathbf{p}, T)}{I_{BB}(\lambda, T)} \leq 1, \tag{1}$$

where $I(\lambda, \hat{n}, \mathbf{p}, T)$ is the spectrum emission power of the thermal emitter per unit area at a given $\lambda$, $\hat{n}$, and temperature $T$, and $I_{BB}(\lambda, T)$ is the spectrum emission power per unit area of a blackbody at the same temperature as the emitter. It is clear that the emissivity is bound between 0 and 1. A perfect thermal emitter will have $\eta = 1$, representing an ideal blackbody, and on the other hand, $\eta = 0$ represents a perfect reflector. Similarly, the absorptivity $\alpha(\lambda, \hat{n}, \mathbf{p})$ determines how much incident light with polarization $\mathbf{p}$ is absorbed in a given $\lambda$ and $\hat{n}$. Kirchoff's law [4] states that in reciprocal systems (composed of linear and time-independent symmetric permittivity and permeability tensors):

$$\alpha(\lambda, \hat{n}, \mathbf{p}) = \eta(\lambda, \hat{n}, \mathbf{p}^*). \tag{2}$$

Kirchoff's law suggests that the thermal emissivity may be controlled by the absorptivity and vice versa. Since most thermal emitters are made of reciprocal materials, this fundamental connection forms the foundation for thermal emission engineering with metasurfaces.

**b. Luminescence**: Light emission from semiconductors, quantum wells, and quantum dots typically originates from the recombination of an excited electron-hole pair, which spontaneously emits a photon [5, 6]. At low excitation levels, the excited state exists for only a short lifetime (∼ps-ns) before decaying into its ground state, emitting a photon in the process. The precise timing of this event is thermodynamically random within the lifetime of the excited state and is independent of other recombination events in the same material. To first order, there are two processes by which an excited electron can emit a photon, namely, stimulated emission and spontaneous emission. Stimulated emission, when a resonant photon

causes an excited electron state to relax and release a photon in phase with the driving light. In the absence of a driving photon, excited electron states still have a finite lifetime and will relax, releasing a photon with no particular phase. This is known as spontaneous emission. Both photon emission rates are described by Fermi's Golden Rule,

$$\Gamma_{i\to f} = \frac{2\pi}{\hbar} |\langle f|\hat{H}'|i\rangle|^2 \rho(E_f), \tag{3}$$

where $\Gamma_{i\to f}$ is the transition probability per unit time from $|i\rangle$ to $|f\rangle$, $\hat{H}'$ is the Hamiltonian describing the electromagnetic field and its interaction with carrier states, and $\rho(E_f)$ is the density of photonic states in the emitting region. In the case of stimulated emission (e.g., during lasing), we can modify the driving field to alter $\hat{H}'$, and thus alter the stimulated emission rate. In the case of spontaneous emission, vacuum fluctuations in the EM field provide a non-zero $|\langle f|\hat{H}'|i\rangle|^2$, and we are left with only one knob to turn: the local density of photonic states.

Metasurface design principles for describing the interactions with coherent light sources (lasers) leverages the coherent nature of the electromagnetic scattering process. We control this scattering process using the metasurface resonances defined by either the geometry (size and shape) or refractive index of the resonators to directly influence the spatial phase, amplitude and polarization properties of light. While this approach can shape the interactions with coherent light sources, it fails to capture the emission properties of emitters embedded within a metasurface. However, the metasurfaces resonances not only help shape the scattering properties but also provide us with a handle to control the local density of photonic states. The same optical resonances within the metasurface now shape the emission profile, by determining the lifetime of the excited state and the probability of emission in a particular direction (or momentum). Using the dispersion relation, $E(k)$, we can rewrite $\rho(E_f)$ as $\rho(k_f)$. A key concept in controlling spontaneous emission in PL is the Purcell factor, which quantifies the enhancement of the emission rate due to an altered photonic environment, such as a resonant cavity or metasurface. The Purcell factor is given by:

$$F_P = \frac{3}{4\pi^2}\left(\frac{\lambda}{n}\right)^3 \frac{Q}{V}, \tag{4}$$

where is the $\lambda$ wavelength of emission, $n$ is the refractive index, $Q$ is the quality factor of the cavity (metasurface), and $V$ is the mode volume. A high Purcell factor leads to enhanced spontaneous emission rates, improving quantum efficiency and enabling directional emission control.

Thus, metasurfaces can be used to shape the energy and the momenta of spontaneously emitted photons. The efficiency of this control is measured in various ways. Directivity is usually defined as intensity emitted at the desired momentum (or, equivalently, angle) over average intensity emitted into all momenta/angles. Emission enhancement is usually defined using the ratio of charge carriers injected (or excited, in the case of PL) to photons exiting the device, i.e., external quantum efficiency (EQE).

**c. Quantized Emission**: Here, we focus on quantum emission from two primary sources: single-photon emitters, such as semiconductor quantum dots and color centers, and two-photon sources, such as spontaneous parametric down-conversion (SPDC). The single-photon emitters follow the principles previously described in the luminescence section with the exception that the photons are emitted in a quantized manner due to three-dimensional confinement of the emitters.

In SPDC, a pump photon is down converted into two daughter photons (a biphoton) after interacting with a second-order nonlinear ($\chi^{(2)}$) material. The two daughter photons are called signal and idler. At the beginning of the nonlinear interaction, both signal and idler photons are in their vacuum states, and the down-converted photons are generated by spontaneous emission. More specifically, when the pump laser of frequency $\omega_p$ enters the nonlinear crystal, the nonlinear susceptibility couples the pump field and the signal field (in the vacuum mode) at frequency $\omega_s$ to produce a nonlinear polarization that oscillates at the frequency $\omega_i = \omega_p - \omega_s$. In its turn, the nonlinear polarization acts as the source of a wave oscillating at $\omega_i$, the idler frequency. Unlike the spontaneous processes described above, SPDC is a coherent process because the individual dipoles induced in the matter radiate in phase. Since SPDC relies on the parametric amplification of the zero-point vacuum field, it is a relatively weak process. In a similar manner as for

Luminescence (see Eq. 3), the rate of biphoton creation can also be calculated using Fermi's golden rule, c.f. Ref. [7].

For SPDC to occur in a $\chi^{(2)}$ material, momentum conservation (or phase matching as known in classical nonlinear optics) and energy conservation conditions must be satisfied. The former is essential for efficient conversion of pump photons into biphotons, and different techniques have been developed to this end. In the case of ultrathin films and metasurfaces, the longitudinal component of the momentum (wavevector) mismatch is relaxed [8] due to their slim profile. Because of that, SPDC from ultrathin films is ultrabroad in frequency [9] and angles of emission [10]. In other words, the zero-point vacuum field seeds SPDC uniformly over the wavelength-angular spectrum. In the case of metasurfaces, the situation is slightly different. Here, resonances enhance the zero-point vacuum field only around the resonant wavelength. Thus, depending on the type of resonant mode, the wavelength spectrum of SPDC may be narrow (high quality factor) or broad (low quality factor). In a similar manner, the type of resonance also selects the range of angles of emission. More generally, the resonance mode can shape the spectrum, angle of emission, polarization state, among other degrees of freedom of the emitted radiation.

## Engineering Thermal Emission with Metasurfaces

Thermal emission is spontaneously produced by objects at temperatures above absolute zero, resulting from the intrinsically fluctuating electromagnetic fields within the materials. The ability to engineer the thermal emission is vital to many technological breakthroughs, including energy harvesting [11, 12], thermal camouflage [13], passive radiative cooling [14], and gas sensing [15]. In contrast to laser light, which has been widely developed using various techniques, thermal radiation is incoherent and poses additional challenges in tuning its properties. It has been established the presence of symmetries in the system imposes direct constraints on $\eta(\lambda, \hat{n}, \mathbf{p})$ and $\alpha(\lambda, \hat{n}, \mathbf{p})$. Breaking the geometric and non-geometric symmetries in metamaterials offers a pathway to control thermal radiation [16, 17]. The breakthroughs in engineering thermal emission have been achieved in the past decade with the swift growth of nanofabrication technologies. Thermal emission can be readily tuned by carefully structuring the unit cell of metasurfaces to obtain the desired wavelength, bandwidth, polarization, and emission direction.

There are two fundamental challenges in controlling the properties of thermal radiation. First, thermal radiation has a broad spectrum, whereas photonic elements typically work within a narrow spectral range. Second, because many materials rapidly lose stability at high temperatures, the library of materials for thermal photonics is limited. In the last decade, tremendous gains have been made to overcome these issues by adopting photonic nanostructures for thermal photonics, including metamaterials, metasurfaces, photonic crystals, and subwavelength structures [18, 19, 20, 21, 22, 23]. Here, we review the recent advancements in the development of thermal metamaterials to achieve spatial, temporal, and spin coherence (Fig. 1). We further discuss the emerging field of thermal metamaterials for infrared machine perception.

### Controlling Spatial Coherence

The spatial coherence of thermal radiation is key to realizing applications such as thermal holography [24] and thermal focusing [25]. Breaking the spatial isotropy of a system provides a pathway to define the spatial coherence (directionality) of thermal emission [18, 26, 27]. In a seminal work, Greffet et al. [28] demonstrated that adding a periodic microstructure in silicon carbide (SiC) produces a coherent infrared source with well-defined symmetric radiation directions. In such metamaterials, the periodic microstructure induces wavevector-selective resonant excitation of surface phonon polaritons, resulting in significant angular-dependent absorptivity. Spatial anisotropy can also be created through circular concentric grooves. By exciting the surface plasmon polaritons in Tungsten and Molybdenum-based circular concentric grooves, Park et al. [29] have demonstrated a highly directional narrowband infrared emitter. Periodic perturbations cause metasurfaces to behave like resonant metagratings with discrete diffraction orders. The emission in grating structures is symmetric around positive and negative angles ($\theta$ and $-\theta$). It has been recently demonstrated that breaking mirror symmetry enables resonances to have different

radiation decay rates than symmetric output ports, resulting in asymmetric directional control [26] over the thermal emission (see Fig. 2(a)).

A paradigm shift in controlling the spatial coherence of thermal radiation was achieved with the introduction of epsilon-near-zero (ENZ) materials [30, 31, 30, 32, 33, 34]. Xu et al. [35] designed a gradient ENZ metamaterials to obtain the directionality of thermal emission over a broadband spectrum. These structures are designed to have vanishing permittivity at a selected range of frequencies varying along a spatial gradient. This gradient ENZ metamaterial supports a broad spectrum of leaky modes that couple to free-space propagating modes at almost identical angles of incidence throughout that bandwidth. Thus, it is possible to realize a broadband directional thermal emitter (Fig. 2(b)) with an angular range regulated by the total thickness of the film. The thermal emitter based on ENZ films can also be engineered to extend into the entire atmospheric window. Ying et al. [36] developed a metasurface on a metal consisting of top ENZ films, bottom ENZ films, and a dielectric gap. The emitter exhibits strong *p*-polarized thermal emission throughout the whole 8–14 $\mu$m wavelength range at specific directions.

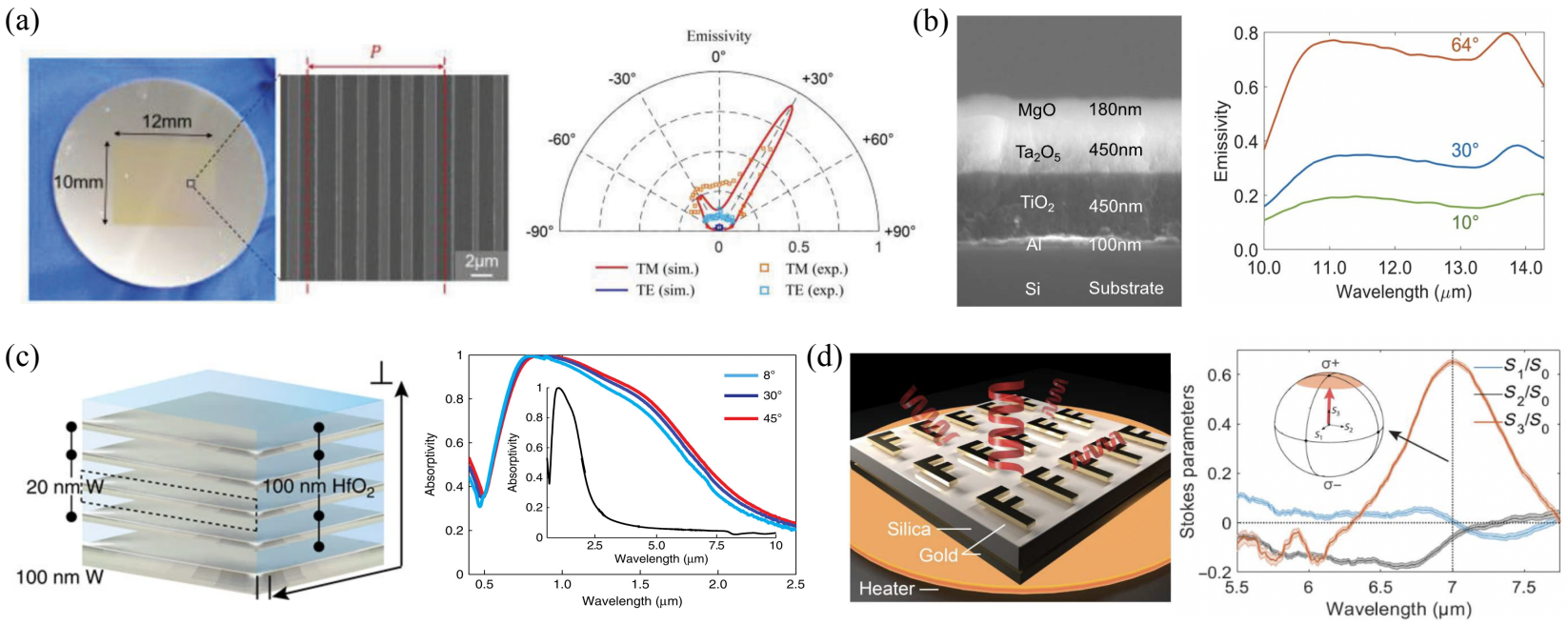


Figure 2: (a) Spatially coherent thermal emission of a metagrating structure with broken mirror symmetry at wavelength 12.6 $\mu$m. (b) Broadband directional thermal emission from a gradient epsilon-near-zero metamaterial. (c) The absorbtivity spectrum of a refractory W-$HfO_2$ metamaterial. (d) The stoke parameters that characterize the spin polarization of thermal emission from a symmetry-broken metasurface with F-shaped meta-atoms. Figures adapted from (a) Ref. [26] © 2023 Wiley-VCH GmbH, (b) Ref. [35] © 2021 American Association for the Advancement of Science, (c) Ref. [37]. CC BY 4.0., (d) Ref. [22] © 2023 American Association for the Advancement of Science.

## Controlling Temporal Coherence

The temporal coherence of thermal radiation is directly related to its spectral bandwidth. This can be demonstrated by applying the convolution theorem, which connects the auto-correlation function to the Fourier transform of the thermal emission spectrum. A popular technique to attain temporal coherence is by designing a metamaterial composed of a metallic mirror, and metallic meta-atoms separated by an insulating spacer layer [38]. Such a metasurface yields emissivity close to unity within a selected spectral bandwidth. Even smaller spectral bandwidths have been demonstrated by fabricating photonic crystals on top of multiple quantum wells [39]. The emissivity of such a device can be increased by combining the intersubband transitions in quantum wells and photonic modes in photonic crystals. These strategies effectively achieve temporal coherence in the mid-wave (MWIR) and long-wave infrared (LWIR) regimes. To expand the capability of temporal coherence in the near-infrared regime, Asano et at. [40] designed nanostructured semiconductor thermal emitters. In these emitters, electron thermal fluctuations are first limited to the higher-frequency side of the spectrum, above the semiconductor bandgap, and then amplified by the photonic resonance of the structure. This double-resonance technique yields selective

thermal emission even at shorter wavelengths.

All of these metasurfaces have been developed to achieve the desired temporal coherence, either through material or structural design. Recent advances in the application of deep learning algorithms for metamaterial design have provided a broad foundation for wavelength-selective thermal emitters that go beyond multilayer structures [41]. Deep learning algorithms can autonomously identify appropriate materials from a material library while simultaneously optimizing structural parameters for the desired emissivity spectra.

Gratings, thin film resonances, and photonic crystals used to spectrally control thermal emission frequently require surface lithography, resulting in significant angle dependence. To overcome this, Dyachenko et al. [37] developed a refractory W-$HfO_2$ metamaterial, which utilizes the material properties to control the thermal emission, instead of resonance or interference effects. In such metamaterials, selective enhancement and suppression of near-infrared thermal emission can be realized by tuning the ENZ frequency and the corresponding optical topological transition. This approach provides a pathway to engineering a nearly omnidirectional and spectrally selective thermal emitter (Fig. 2(c)).

## Controlling Spin Coherence

Spin-polarized thermal light sources can be used to design passive infrared beacons for outdoor settings [42], infrared chiral spectroscopy [43], and thermal imaging polarimetry in low-visibility conditions [44]. Thermal metasurfaces can also provide an avenue for both spin coherence and polarization selection. Early works in this domain were focused on obtaining linearly polarized thermal emission. Schuller et al. [45] demonstrated that thin SiC nanorods can be engineered to support TE and TM polarized modes that are well-separated in wavelength. Mason et al. [46] developed a TM-polarized thermal metasurface composed of gold grating on a spin-on-glass layer integrated with a thick gold mirror. Here, the polarized emission is induced by the antiparallel surface currents in the metal mirror and grating. In recent years, developing systems with spin polarized thermal emission has also gained significant importance.

Spin polarized thermal emission is a distinct phenomenon observed in condensed stars [47, 48], that can result in the discovery of strong magnetic fields, and even suggest the presence of life [49, 50]. An external magnetic field or intrinsic nonreciprocity in bianisotropic media can generate spin polarized thermal emission. Magneto-optical materials [51, 52, 53], Weyl semimetals [54, 55, 56], and topological insulators [57] are all predicted to exhibit chiral thermal emission upon breaking the time-reversal symmetry through an external magnetic field.

In metamaterials, spin polarized radiation patterns can be obtained at oblique angles by breaking the inversion symmetry even without any external magnetic field. Inversion asymmetric metasurfaces have been observed to display spin split emission bands, and this phenomenon has been termed as the optical Rashba effect [58]. However, in such structures, the net helicity is zero due to anti-symmetric spin patterns. Breaking the mirror and inversion symmetries simultaneously removes all constraints, allowing control over both the temporal and chiral characteristics of the emitted photons. Based on this symmetry-breaking strategy, Wang et al. [27] designed a chiral metasurface, and observed asymmetric spin patterns (Fig. 2(d)) and nonvanishing optical helicity, reaching 39% of the fundamental limit.

Unlike mechanisms involving geometrical symmetry engineering, coupled nonequilibrium sources offer an alternative mechanism to generate spin-polarized thermal emission. Khandekar et al. [59] predicted this phenomenon on a pair of subwavelength coupled antennas with different temperatures. In such a system, changing the temperatures of the antennas can reverse the handedness of the emitted light, allowing the polarization state to be reconfigured.

Beyond symmetry-broken local metasurfaces, nonlocal thermal metasurfaces [60] have recently received significant attention for their ability to achieve spin-selective, unidirectional, focused emission while controlling the angular orbital momentum of thermal beams [61, 62]. These designs employ quasi-bound states in the continuum (BICs) supported by a periodic array of pillars, whose in-plane long-range order permits coherent thermal emission. The two orientation angles in nonlocal metasurfaces relative to the fixed lattice can be adjusted to achieve full control over the geometric phase and the degree of circular polarization [63]. Von Neumann and Wigner first predicted the BICs phenomenon in 1929 [64], and today, the topological interpretation of BICs remains an active area of research [65]. Investigating BICs in nonlocal metamate-

rials could bridge the fields of topological physics and thermal photonics, enabling topologically tailored radiative heat transfer.

### Thermal Metasurfaces for Infrared Machine Perception

Thermal imaging operating within the atmospheric transparency window, has numerous applications in space, defense, and agricultural technologies. Leveraging the ubiquitous thermal emission presents novel avenues for scalable perception. However, objects and their surroundings continuously emit and scatter the thermal radiation, resulting in textureless images [66, 44]. This has made it challenging to implement applications like thermal ranging, which is necessary for autonomous navigation.

Recent advancements in heat-assisted detection and ranging (HADAR) [67] have demonstrated that integrating spectral-resolved thermal imaging with machine learning empowers machine perception in pitch darkness as if it were daylight. This HADAR technique is based on a neural network model that was extensively trained with thermal data from an infrared camera to determine the temperature, emissivity, and texture of each object in an image (Fig. 3(a)). The HADAR technology can transform machine perception in low-visibility conditions.

The widespread use of such machine learning algorithms has increased the demand for high-resolution, information-rich image data, especially in MWIR and LWIR. Spectral and polarimetric imaging systems based on meta-optics have shown the potential to fulfill the data needed for image processing in the visible spectrum. However, combining meta-optics with infrared thermal imaging is still largely unexplored [69]. To address this, Wang et al. [68] developed a spinning-metasurface-based spectro-polarimetric stack that provides exceptional spectral resolution in LWIR across diverse materials and enabling applications such as material classification (Fig. 3(b), (c)). This technique can achieve three times greater accuracy for machine vision tasks than traditional panchromatic thermal imaging. In the future, such imaging platforms can facilitate the real-time capture of videos, resulting in the widespread adoption of HADAR technology for infrared machine perception.

### Thermal Metasurfaces for Passive Radiative Cooling

A prospective solution to the problem of global warming is passive radiative cooling through thermal metasurfaces, an emerging technique that can reduce temperatures below room temperature without using outside energy. Radiative cooling can be achieved by passively dissipating heat from Earth into space using thermal emitters engineered to have a high emittance within atmospheric transparency windows ($8-14\,\mu$m and $3-5\,\mu$m), while restricting infrared absorption outside the window.

Raman et al. [14] demonstrated this phenomenon using a multilayer dielectric structure with a silver backing layer. The dielectric layers can selectively emit heat at the targeted mid-infrared wavelengths while collectively enhancing reflection from the sun. This structure reached a temperature 5 $^0$C lower than the air temperature when placed on a rooftop. However, such nanophotonic structures require precise fabrication over a large area, which is difficult to scale up economically. To overcome this challenge, Zhai et al. [70] developed a metamaterial made of a polymer layer with implanted microspheres, constructed on top of a silver layer. By accessing the high-order Fröhlich resonances of the polar dielectric microspheres, these metasurfaces offer broadband emissivity over the whole atmospheric window. This large-scale design provides high infrared emissivity within $8-20\,\mu$m and efficient solar irradiance reflection close to 0.96, allowing for a continuous three-day average cooling power of 110 Wm$^{-2}$. In recent years, hierarchically engineered radiative cooling materials [71, 72, 73] have received a great deal of interest for their ability to produce selective thermal emitters. Li et al. [71] synthesized a polyethylene oxide nanofibre-based film using a roll-to-roll electrospinning technique. This structure was demonstrated to have a high reflectance in the sunlight wavelengths as a result of its disordered photonic structure with many nanofibres, and it emits selectively in the mid-infrared range due to its unique bond vibrations. This opens up new opportunities for the construction of large-scale, high-performance radiative cooling solutions. These successful demonstration of radiative sky cooling illustrates the promise of thermal metamaterials for renewable energy applications.

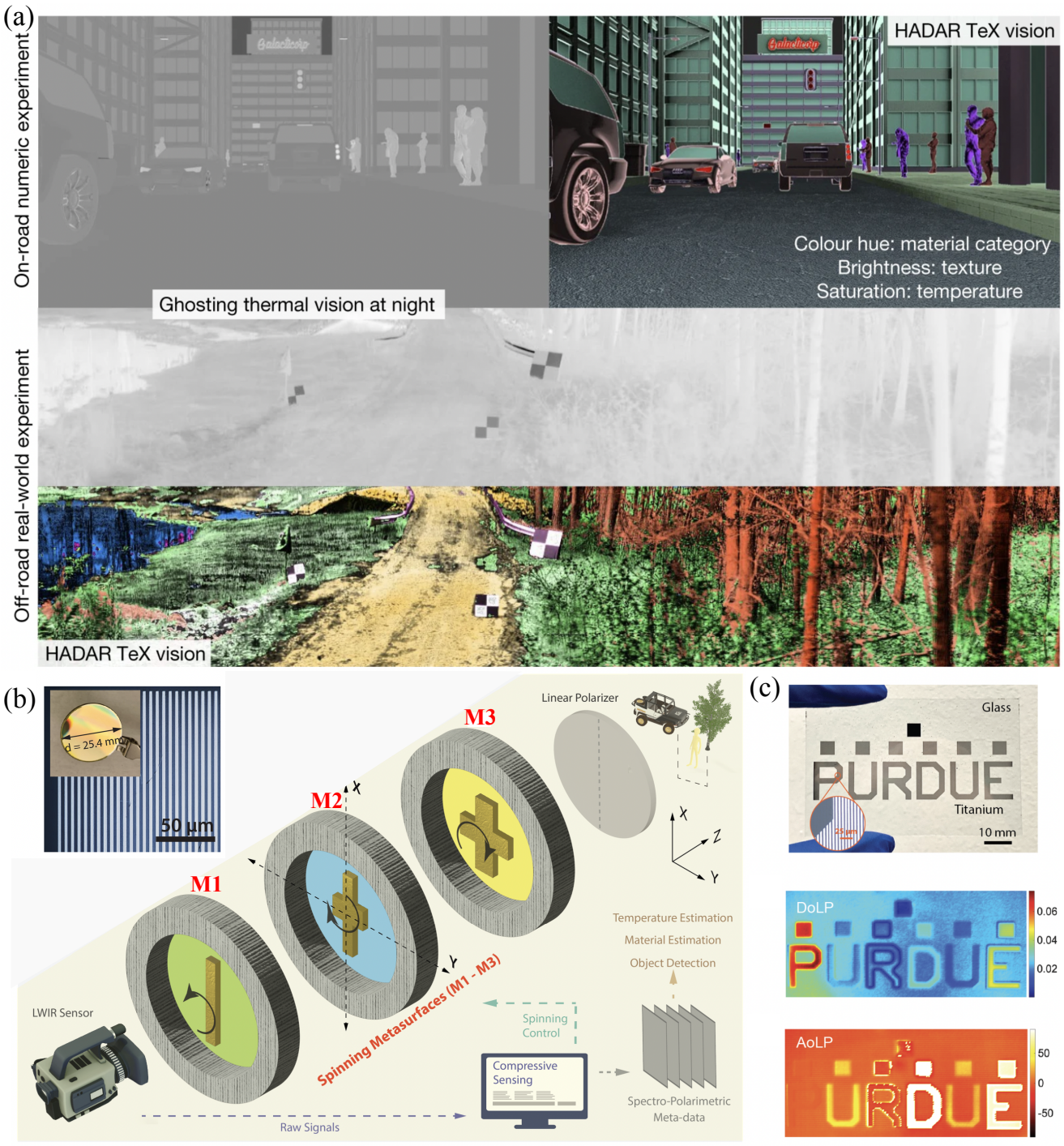


Figure 3: (a) HADAR technology captures heat cubes for hyperspectral imaging, and deconstructs a textureless image using temperature, emissivity, and texture (TeX) decomposition. It is evident from TeX vision experiments that HADAR can perceive textures through complete darkness. (b) Combining compressive sensing reconstruction algorithms with large-area spinning metasurfaces allows for spectrophotometric thermal imaging. (c) An optical image of the imaging target with micro-structures designed to produce unique spectral and polarimetric patterns for each letter. The degree (DoLP) and angle of linear polarization (AoLP) frames reveal distinctive polarimetric signatures for each letter in the images. Figures adapted from (a) Ref. [67], and (b, c) Ref. [68] © 2024 Optica Publishing Group.

## Engineering Luminescence with Metasurfaces

Metasurfaces, through their sub-wavelength array of optical resonators, maximize light-matter interactions modifying the LDOS for embedded emitters leading to Purcell enhancements of emission.[74] The spatial distribution of optical resonances within the metasurface can enhance light emission spectrally, shape the far-field emission directions, and polarize the emission. Metasurfaces offer a unique opportunity to enhance the emission rate and shape the wavefront through spatial engineering of the local permittivity around resonators with embedded emitters. As a result, metasurfaces have recently been employed to enhance and direct photoluminescence (or electroluminescence) from atomic, molecular, and semiconductor emitters, driving an active research area with diverse applications. Due to their low form factor (in terms

of size and weight), metasurfaces have found novel applications in augmented/virtual reality displays [75], nanoscale electric field measurements [76], high-resolution and high-speed LIDAR [77], and qubit manipulation for quantum computing [78]. In many cases, metasurfaces integrated into the far-field of an emissive system [75, 79, 80, 81, 82, 83, 84, 85, 86] can increase collection efficiencies or modify the emitted wavefronts. Here, we focus on research where emitters are positioned within the near-field of a metasurface to modify their spectra, polarization, efficiency, and emitted wavefront. Prior investigations of plasmonic [87], optical antenna [88], and photonic crystal [89] emitters have laid the groundwork for light emission from metasurfaces. Building on these early studies, metasurfaces provide additional degrees of freedom, such as multi-resonance effects, spatio-temporal engineering, and phased-array effects across light-emitting devices, suggesting the potential for holographic control of incoherent light.

## Emission Enhancements and Spectral Engineering

The electric field enhancements associated with a sub-wavelength plasmonically resonant optical antenna have been utilized to spectrally enhance the LDOS of an emitter at the resonant wavelength.[90, 91, 92, 93]. Specifically, the field enhancements in between plasmonically resonant optical antenna (or gaps) elements provide an interesting approach to surpass limitations of individual dielectric resonators [94, 95]. Early work showed that peak emission intensity from conventional blue LEDs (InGaN/GaN quantum wells) can be increased by an order of magnitude by depositing metallic layers (Ag, Al) 10 nm above the light-emitting InGaN layer [96]. For phosphor-based white LEDs, an array of metallic nanoparticles has also shown to increase luminescence intensity [97]. While the electric field enhancements and the modal confinement of the plasmonic reosnances near the edges, corners and gaps between metallic elements can lead to large Purcell factor enhancements, the emitted photons typically face large Ohmic losses or absorption due to the metal itself. Following up on these initial studies on plasmonic light-emitting systems, lower ohmic loss dielectric systems like photonic crystals with embedded emitters were utilized to spectrally enhance the emission (LDOS) with the photonic modes relying on the translational symmetry in the crystal lattice.[98, 99] Photoluminescence from dielectric metasurfaces moved beyond the restriction of translational symmetry within the lattice, with embedded emitters demonstrating increased luminescence intensity by several orders of magnitude [100, 101]. Dielectric approaches enable resonator fabrication directly from emitting semiconductors [102, 2] and Mie resonator approaches are particularly useful for achieving PL enhancements from magnetic dipole emitters [103, 104, 105].

Recent developments in metasurface-enabled spontaneous emission enhancements largely derive from explorations of new classes of materials. Lanthanide-doped up-converting nanoparticles (UCNPs) are of particular interest given the very weak nature of the underlying 4f transitions, see Fig. 4. The nonlinear aspects of up-conversion and the combined importance of electric and magnetic dipole transitions provide opportunities to engineer metasurface effects that go beyond traditional designs [106, 107]. Likewise, chiral metasurfaces have the potential to enhance the manipulation of valleytronic effects within transition metal dichalcogenides (TMDs) [108, 109, 110]. Hybrid organic/inorganic perovskites are another emerging class of metasurface emitter [111, 112]. Like purely inorganic semiconductors, the emitting material can itself be fashioned into a meta-element [113, 114]. Unlike traditional inorganic semiconductors, solution-based synthesis of these materials provides both advantages and challenges for metasurface fabrication [115, 116, 117].

## Wavefront Control

Traditional spontaneous emission sources emit photons across a wide range of angles.[118] Narrowing this emission angle is advantageous as a means of improving collection efficiencies and is significant to the widespread use of inexpensive, incoherent emission sources in applications that currently use coherent sources, such as holographic displays [119] and remote sensing [120]. Control over emission angles has been demonstrated in dielectric [2] and plasmonic [92, 121] metasurface arrays. Even within uniform arrays, modifications to directivity have been achieved by engineering nano-antenna resonances via, e.g., Kerker effects [122, 123] or anapole modes [124], or by engineering more spatially extended metasurface properties

via, e.g., surface lattice resonances [85, 125] or bound-states-in-the-continuum [126, 2]. Directing different emission channels to different output directions is a particularly useful function that can be achieved within uniform arrays [127, 128].

Moving beyond uniform arrays, phased-array designs have the potential to impart generalized PL wavefronts. In these cases, the emission pattern is dictated primarily by interactions between meta-atoms, rather than by the physical parameters of individual meta-atoms. Earliest examples of such phased-array engineering produced asymmetric emission profiles in plasmonic Yagi-Uda antenna arrays [129, 1, 130]. Extending these phase profiles across an entire surface, Iyer et al. [131] demonstrated the steering of spontaneous emission to specific output angles (i.e., unidirectional emission) in metasurfaces consisting of InGaN quantum wells embedded within GaN nanopillars. The metasurfaces were designed around a peak in the unpatterned film's LDOS near the critical angle; a gradient in the transmission phase across the surface redirects the critical angle emission peak towards normal exitance. Focused PL was subsequently achieved in 2D arrays [132] using an equivalent design approach. Exploiting the Pancharatnam - Berry (PB) phase represents another approach for engineering non-uniform phase profiles. Rong et al. [133, 134] were able to utilize PB phase engineering to demonstrate the photonic Rashba effect, whereby emitted photons were split in momentum space according to their spin.

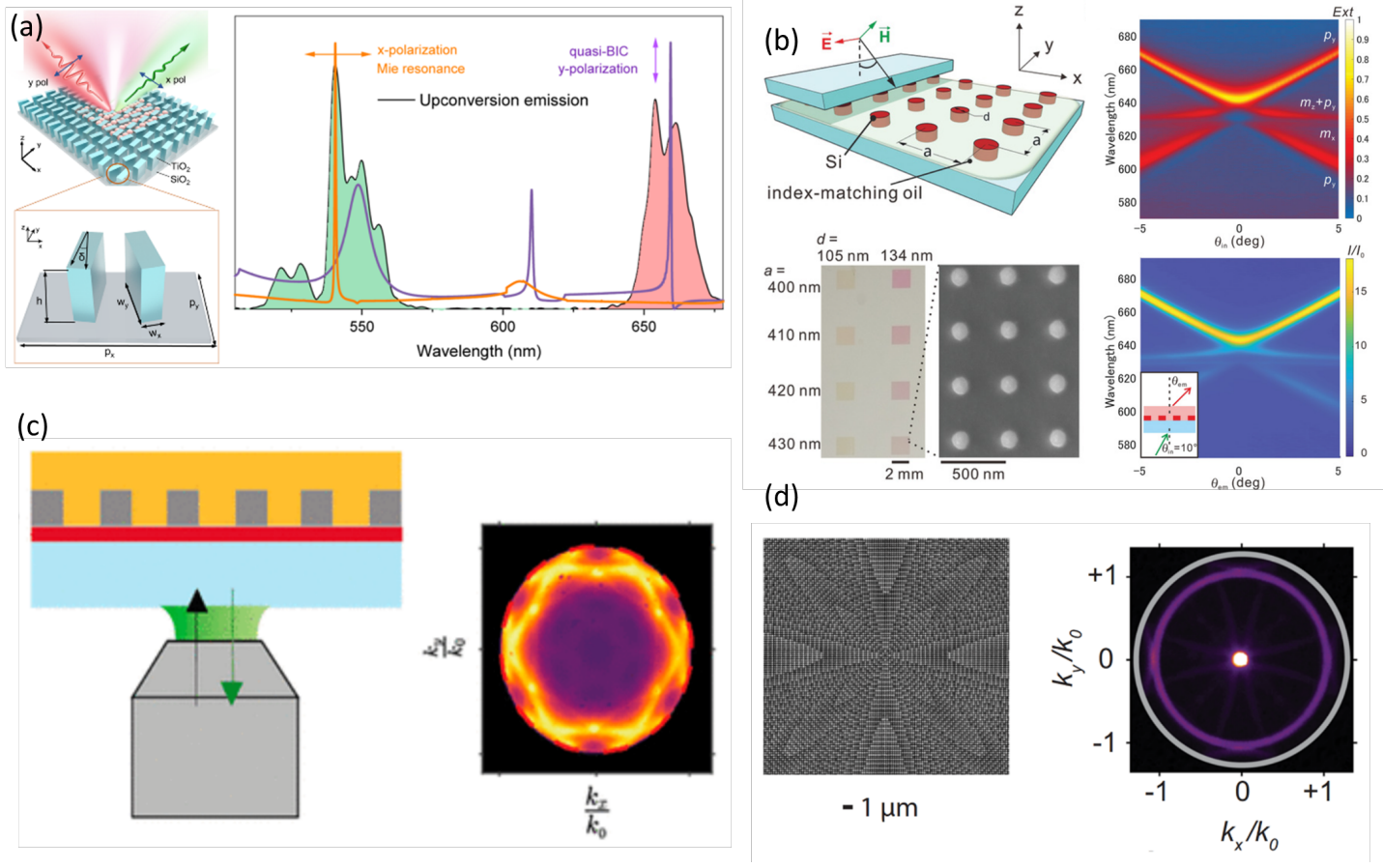


Figure 4: (a) A non-uniform dielectric metasurface integrated with Lanthanide-doped up-converting nanoparticles allows for polarization-controlled enhancement of dual-band upconversion. (b) Directional light emission from a uniform array of dielectric nanodisks engineered to support electric and magnetic Mie surface lattice resonances. (c) A nanopatterned perovskite film (orange) yields directional photoluminescence (PL) emission. (d) A meta-axicon for focusing PL, composed of semiconductor quantum well emitters embedded in nanopillars. Figures (a) adapted from [106] © CC-BY, (b) reprinted from [125] © CC-BY-NC-ND, (c) reprinted from [114] © CC-BY, (d) reprinted from [132] © CC-BY.

## Active Control of Luminescence

Active modulation of incoherent light emission, ranging from simple on-off switches to dynamic wavefront control, is a necessary components to commercialize and extend the utilization of incoherent light sources. LEDs have become the ubiquitous light source of the modern world due to their efficiency of operation compared with traditional incandescent (or thermal) light sources. Decades of research have brought

the internal quantum efficiency (IQE) of LEDs, i.e., the ratio of photons produced per charge carrier injected, to near-unity. However, the external quantum efficiency (EQE), which includes the percentage of photons that escape the LED, is lagging significantly behind [135]. The EQE is primarily limited by the light extraction efficiency from the device due to total internal reflection; the high refractive index of the semiconductor tends to trap photons within the LED structure. Metasurfaces provide a possible solution for simultaneously enhancing photon extraction and engineering the output optical wavefront. Metasurfaces can re-direct the light which would have been trapped in the substrate to out-couple into free-space. Many early demonstrations consisted of passive metasurfaces integrated into the far-field of device structures. For instance, Khaidarov et al. embedded GaP LEDs within a distributed Bragg reflector cavity to suppress off-normal light emission [81]. A Si metasurface integrated atop the cavity subsequently shaped the far-field directivity of incoherent emissions. This design achieved both directionality and vortex beam generation but with a low efficiency of around 20%. A similar design, using an OLED emitter, achieved an efficiency above 40% and deflection angles as wide as 30° [79].

Metasurfaces have also been utilized as an integrated spectral-filter within organic LEDs. Joo et al. designed metasurface back reflectors to selectively and optimally extract red, green, and blue light from a white-emitting OLED, allowing for ultra-high pixel density [75]. Mohtashami et al. demonstrated generalized metasurface phase engineering in GaN/AlGaN quantum well LEDs [136]. Metasurface LEDs showed improved external quantum efficiencies (EQEs) relative to unpatterned devices, demonstrating that metasurface fabrication is compatible with high EQE metal-free semiconductor LEDs.

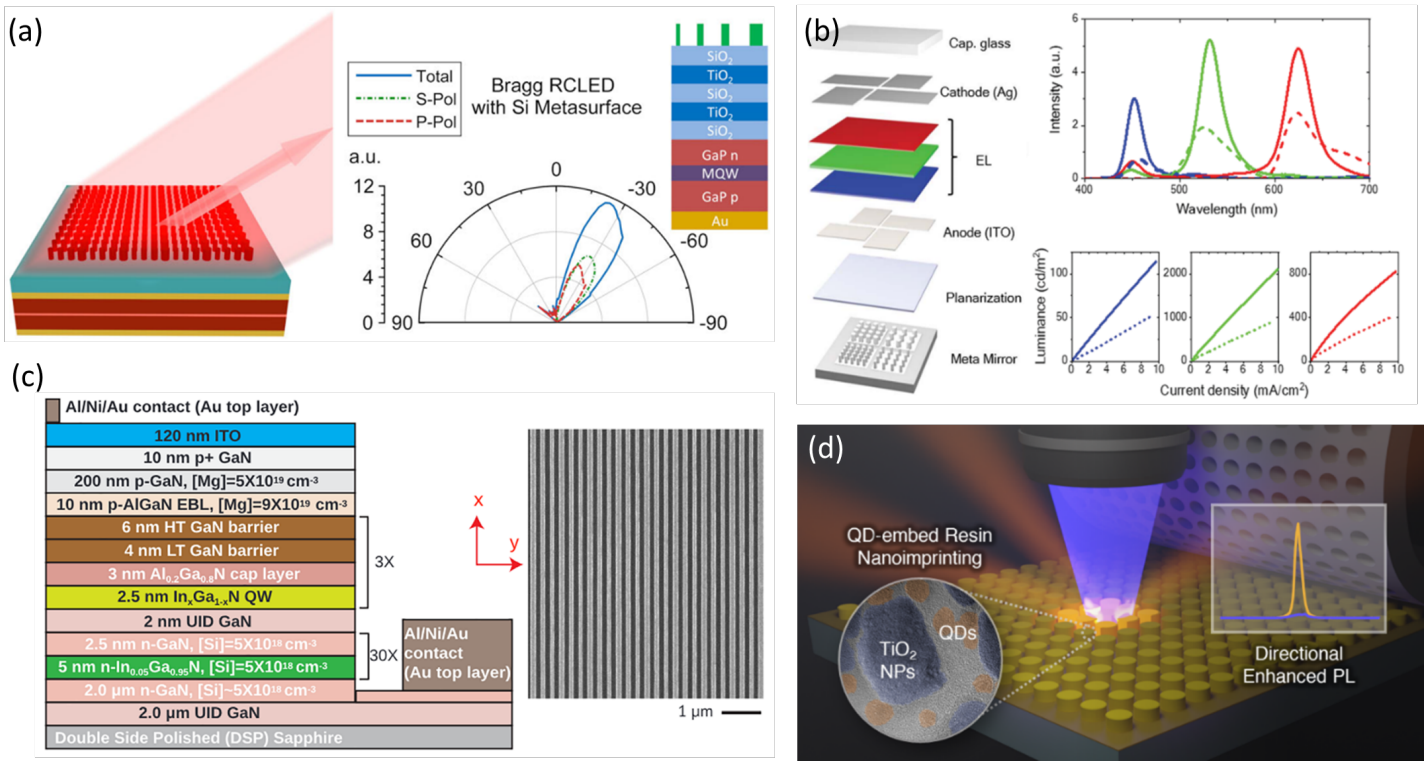


Figure 5: (a) Metasurface-mediated directional electroluminescence (EL) in a LED. (b) A metamirror integrated into a white-light OLED platform allows for optimal extraction of red, green, and blue light in a high-density pixel. (c) A design allowing for a 1-d metasurface embedded with electroluminescent semiconductor emitters. (d) Nano-imprint lithography presents a method of quickly fabricating large numbers of wide-area luminescent metasurfaces. Figures (a) adapted with permission from [81] © 1999-2024 John Wiley & Sons, Inc or related companies, (b) adapted with permission from [75] © 2024 American Association for the Advancement of Science, (c) reprinted with permission from [136] © 2023 American Chemical Society, (d) reprinted with permission from [137] © 2024 American Chemical Society.

Despite this progress, the vast majority of metasurface designs were static in nature, implying that steering spontaneous emission to various angles at various intensities required multiple metasurface designs and fabrication steps. A recent breakthrough from Iyer et al. [138] demonstrated that arbitrary control of spontaneous emission can be achieved via reconfigurable metasurfaces, using a single design. The operating principle of a reconfigurable metasurface is that a spatially varying refractive index profile can steer spontaneous emission to arbitrary angles using momentum matching principles, see Fig. 6 (a).

Spatially varying refractive index profiles were achieved in this work by introducing spatially varying optical pump patterns, which induce local free carrier concentration changes. This principle was demonstrated on a GaAs metasurface with InAs quantum dots embedded within $In_{0.15}Ga_{0.85}As$ quantum wells. Imposing pump patterns with varying grating orders (periodicities), unidirectional steering of spontaneous emission was controlled over a 70° field of view. Furthermore, changing the sign of the grating order directly changed the sign of the steering angle, providing a large degree of control over the spontaneous emission from the metasurface, see Fig. 6 (b).

However, while a systematic change in pump patterns can yield arbitrary angle control, it is unclear whether the imposed pump pattern is optimal to steer emission to a specific angle. Designing optimal pump patterns that steer emission maximally to a desired angle, and minimally to other angles, i.e., have high directivity, is non-trivial. The design space of possible pump patterns is the space of patterns that can be imaged onto a spatial light modulator, i.e., a design space of dimension $\sim 8$ million. Exploring this space of pump patterns is impossible with high-throughput experiments, and current modeling and simulation tools do not capture spontaneous emission accurately enough to be used as design aids. Thus with limited human intuition, recent work has focused on combining machine learning with high-throughput experiments to design pump patterns that optimally steer spontaneous emission from reconfigurable semiconductor metasurfaces [139]. Specifically, a combination of generative models and Bayesian optimization were used to identify pump patterns that optimally steer spontaneous emission to specific angles, see Fig. 6 (c). Generative models such as variational autoencoders (VAEs) [140] were used to generate a wide variety of pump patterns, with a range of local slopes (grating orders) far beyond the grating order based pump patterns explored in [139]. VAEs, during the training phase, encode training data (pump patterns) into a low-dimensional latent space, such that the high-dimensional pump pattern can be reconstructed accurately from the latent space, while learning a latent space as a Gaussian distribution close to a zero-mean unit covariance Gaussian distribution $N(0, I)$. Sampling the learnt latent space results in arbitrary pump patterns. However, sampling the latent space often results in pump patterns that do not direct emission optimally, and thus, Bayesian optimization was used to search the latent space of the VAE and find pump patterns with high directivity (maximal emission at the desired angles and minimal emission at other angles). The discovered pump patterns had directivities an order of magnitude greater than sawtooth based pump patterns from prior work, see Fig. 6 (d) and Ref. [139, 141].

### Current Challenges

While embedding emitters within the metasurface has proven to be a successful strategy for achieving control over spontaneous emission, several challenges remain on the path towards arbitrary luminescent wavefront control. At a fundamental level, the primary obstacle is maximizing the fraction of light which is emitted via metasurface-mediated channels. In most cases, metasurface wavefront-transformers are superimposed on a luminescence background that only manages to re-direct a small fraction (<50%) of total light emission. Advanced simulation-enabled designs and experimental refinements could maximize the coupling between metasurface emission channels and the luminescent background. Various studies highlight the importance of starting with an LDOS pattern which has enhanced directional emission before imposing metasurface phase profiles; suggesting an important pathway to improving performance. At a practical level, integration of optical and electronic wave-function simulations with scalable fabrication methods is a critical challenge for achieving practical devices. Similarly, there remains a gap in our understanding of how arbitrary spatial-phase profiles on a metasurface can control the far-field directivity of luminescence.

**a. Full wave simulation of light-emitting metasurfaces**: Designing light-emitting metasurfaces present fundamental challenges relative to traditional passive metasurfaces. Consider the case of a simple phased-array metasurface designed for unidirectional output wavefronts. In a passive implementation, a coherent incident wavefront (typically a single plane wave) is assumed, and the output wavefront can be determined from a single simulation. In the equivalent luminescence experiment, dozens or hundreds of simulations are needed to simulate the incident "wavefront": an incoherent sum of plane waves distributed across a range of angles or momenta (or equivalently an incoherent assembly of local dipole emitters). As

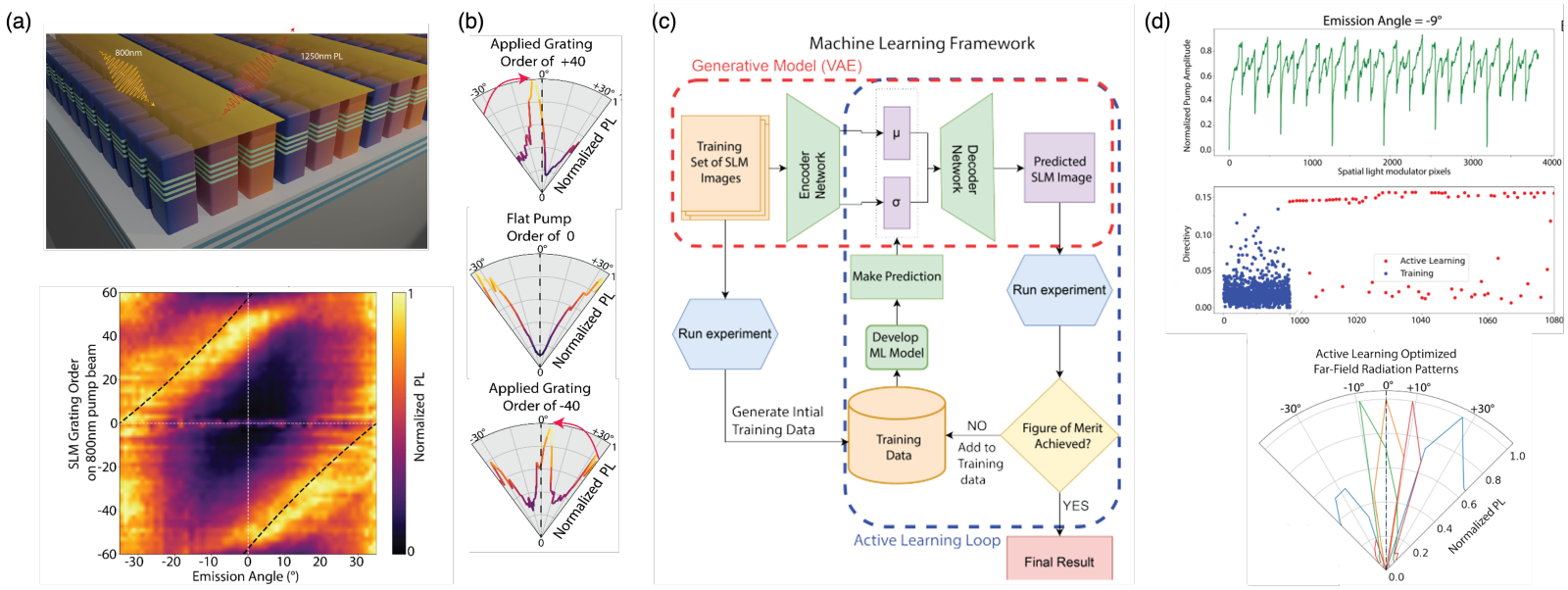


Figure 6: (a) (top) Schematic of a GaAs metasurface with an imposed pump resulting in luminescence from the embedded InAs quantum dots (bottom) Luminescence across a 70°angle, by varying the grating order of the pump pattern projected on the metasurface [138] (b) Examples of emission directivity for three grating order based pump patterns imposed on a GaAs metasurface (c) Machine learning framework to discover pump patterns with optimal emission directivity. The framework involves a generative model (VAE) to generate arbitrary pump patterns, and Bayesian optimization to discover optimal pump patterns in the search space defined by the latent space of the trained VAE [139]. (d) (top) Illustrative result, showing the optimal pump pattern found for one emission angle. (below) Luminescence obtained from using pump patterns found by the machine learning framework, across multiple emission angles. Panels (a) and (b) are adapted from [138] CC BY-NC-SA 4.0. Panels (c) and (d) are adapted from [139] CC BY-NC-SA 4.0.

such, computationally efficient simulations are needed.

Simulations of periodic structures are most-common and generally fall into two categories, LDOS calculations [142, 143, 107] or reciprocity-based approaches based off e.g., finite-difference time-domain (FDTD) or rigorous coupled-wave analysis (RCWA) simulations [144, 145, 146]. In either approach, researchers are utilizing recent advances in artificial intelligence and machine learning to efficiently comb parameter space determine optimal metasurface designs [139, 147]. Although most simulations can only calculate relative (e.g., angle-dependent) emission intensities, a recently developed Local Kirchoff's Law formulation offers an approach for calculating absolute metasurface emission intensities [121].

Because simplifying boundary conditions can no longer be used, efficiently simulating non-periodic luminescent structures such as metasurface lenses or holograms remains a significant challenge that hinders design and optimization. Here, developments in passive metasurface simulation may be particularly instructive. One approach, for instance, is to divide the metasurface into smaller regions, each of which contains a metasurface design that can be solved analytically, using Mie scattering theory, etc., and then to combine the analytical results from each region in order to effectively and efficiently simulate the whole arbitrary metasurface [148].

**b. Energy efficiency electroluminescent devices**: A significant challenge with the electroluminescent metasurfaces is integrating electrical and optical functionality while retaining the ability to estimate the quantum efficiency of the device. For instance, integrating metasurface functionality into metal back electrodes is a relatively straightforward approach suitable for OLEDs, but incompatible with high-EQE semiconductor LEDs that deliberately avoid having metal electrodes within the emitting aperture of the device. The nanoribbon approach employed by Mohtashami et al. [136], while promising, is limited to 1D metasurface profiles. Hole-array metasurfaces may offer an alternative approach [149, 150, 151] leveraging development of semiconductor photonic-crystal based surface emitting lasers [152]. Ultimately, an optoelectronic design paradigm that can take advantage of the dynamic spatio-temporal phase profiles of photo-luminescent metasurfaces to develop high-EQE metasurface-LEDs remains an open challenge.

**c. Cheap, High-Throughput Fabrication**: A metasurface's functionality is defined largely by the spatial distribution of the sub-wavelength scale resonant features. Unlike thermal emitters, patterning a

metasurface to shape visible emission generally cannot be done with visible-wavelength photolithography. Often, electron beam lithography is necessary to define the nano-scale spatial features which is reduces the throughput and remains costly. To realize luminescent metasurface applications, nano-fabrication methods of high-throughput, low-cost manufacturing must be employed. Deep-UV lithography uses light with a wavelength of either 193 nm or 248 nm, allowing for smaller feature sizes than visible lithography without surpassing the diffraction limit. This method was used to fabricate a large area, i.e. approximately 60 $cm^2$, plasmonic metasurface with walls as thin as 90 nm and pillars (holes) as tall (deep) as 159 nm (210 nm) [153]. Nano-imprint lithography (NIL) can be used as an extension of deep-UV or e-beam lithography to recreate these nano-scale patterns in mass. NIL has been successfully demonstrated for a variety of luminescent metasurface designs, including coated UCNP emitters [154], embedded QD emitters [137], and a novel approach involving a metasurface "sticker" on polymethylmethacrylate (PMMA) embedded with dye emitters [155].

To summarize, metasurfaces can passively enhance and actively direct spontaneous emission from various photoluminescent sources and electroluminescent devices.To make a significant impact on fields such as lighting or augmented reality/virtual reality displays, we have outlined a few challenges that need to be tackled, including achieving high degrees of metasurface-mediated emission through more sophisticated simulation and design, integrating metasurface functionality within electrical devices, and developing scalable fabrication approaches. The current rate of innovations within the field of nano-fabrication process control and integrated optoelectronic simulation methodologies provides a promising pathway to the overcome the challenges that are seemingly limiting the expanding influence of light-emitting metasurfaces.

## Engineering Quantum Emissions with Metasurfaces

Generation and manipulation of individual photons are necessary functions required for all quantum optical systems, including meteorology [156], computation and cryptographical applications. There has been extensive research delving into practical solutions, as discussed by Shields et al., where the ideal quantum light sources operate by producing on-demand entangled photons [157, 158]. In this section we will focus on two of the major quantum light sources which are inherently spontaneous: isolated quantum emitters (like quantum dots and color centres) and the spontaneous parametric downconversion (SPDC) process in nonlinear materials. These quantum light sources possess highly desirable attributes while metasurfaces offer unique opportunities for enabling more efficient operation of these sources and for realizing novel functionalities by modifying the generation of quantum light.

### Quantum emitters embedded in metasurfaces

Isolated sources of quantum light (e.g. color centers in diamond, silicon etc, colloidal and semiconductor quantum dots) are ideally suited for use in quantum information systems [159, 160, 161, 162, 163, 158, 164, 165, 166]. Semiconductor quantum dots and color centres in diamond and silicon are of particular interest owing to the potential for direct monolithic integration with photonic devices. Epitaxially-grown quantum dots represent one of the most established solutions for quantum emitters, exhibiting highly desirable properties, such as high levels of brightness [167], on-demand operation capabilities [168], and photon indistinguishability [169]. However, even the most established sources of quantum light still lack the performance needed for quantum information systems [156]. Metasurfaces can provide a great solution for improving their performance and making them more suitable for quantum applications. In the case of quantum dots and color centers, metasurfaces can mitigate two severe limitations of these quantum light sources: the spontaneous emission rate is low for quantum information applications due to the low intrinsic relaxation rate, and the emission directivity is poor. Furthermore, for quantum emitters embedded in a high refractive index material, only a small number of generated photons couple out to free space whilst the majority remains trapped in the high-index material due to total internal reflection.

Metasurfaces have provided a unique opportunity to mitigate the low outcoupling efficiency while leveraging the embedded nature of quantum dots and color centers. Early demonstrations of engineered quan-

tum emitter's environment with the end goal of creating high-performance single-photon sources were realized using colloidal quantum dots integrated with photonic crystals by Lodahl et. al. in 2004 [170]. This result prompted the development of photonic crystal cavities with embedded epitaxial quantum dots and it was successfully demonstrated by Hennessy et. al in 2007 [171]. Additional functionalities were developed in the following years with the dynamic control of quantum dot emission demonstrated by Luo et. al in 2019 [172]. Plasmonic antennas played a groundbreaking role in modifying the environment of the single-photon emitter and thus its emission properties. A nano-antenna coupled to a nearby quantum dots was demonstrated by Curto et. al. and Livneh et. al. to improve the emission directionality and increase the spontaneous emission rate using colloidal quantum dots [173, 174], and then a few years later by Pfeiffer et. al. using epitaxial quantum dots with a high precision alignment process [175]. A wide range of alternative methods for enhancing the emission of quantum emitters has been developed in recent years: Claudon et. al. used nanowires to enhance the emission from quantum dots [176, 177]; Sommaschi et. al. embedding epitaxial quantum dots within micropillar cavities [178], Faraon et. al. used ring resonators [179] and Liu et. al leveraged circular-shaped Bragg grating reflectors [180].

In parallel, in addition to traditional epitaxial quantum dot growth techniques, which can experience limitations in growing low density quantum dots, alternative growth methods, such as local droplet etching (LDE) initially proposed by Watanabe et. al., have become more mature demonstrating high quality, low density quantum dots growth in more recent years [181, 182, 166, 183, 184].

While the approaches described above have demonstrated many effective solutions, they also shed light on the reliance of these solutions on nm-scale precision alignment of the quantum emitter location relative to the photonic nano structure [191]. The reliance on precision alignment poses severe scaling limitations and impedes development of systems where many single photon sources are required within a single chip. Furthermore, often the photonic mode in the nanoscale structure must be spectrally aligned to the emission wavelength of the source [192]. The wavelength and position alignment requirement can be relieved by using metasurfaces with periodic arrays of resonators supporting photonic modes with relatively wide resonances. Such metasurfaces can permit scalable platforms with of monolithically integrated single photon sources [187].

Dielectric metasurfaces in particular are a promising solution for generation and controlling of light emission from monolithically integrated quantum dots and color centers [193]. As discussed in Section 2, these metasurfaces have been already used with large-density quantum dots ensembles, demonstrating significant manipulation of emission, including: improved outcoupling, brightness[194, 100, 195, 196], and dynamic control of emission properties such as directionality [138]. These investigations laid the foundation for expanding the use of metasurfaces for enhancing the outcoupling efficiency and controlling the directionality for emission from individual quantum dots (Fig. 7d) [188, 189, 197].

The concept of coupling a single emitter to Mie modes in a dielectric resonator was explored by Khoury et. al. using impurities in silicon (Fig. 7b) [186]. It was expanded by Iyer et. al. to use with epitaxial quantum dot systems, experimentally achieving an order of magnitude enhancement of the outcoupling from a single quantum dot embedded in a Huygens' Mie metasurface [188]. This metasurface design uses the two fundamental Mie electric and magnetic dipole modes, to control the directivity of the emission process. At the same time, the uniform spatial profile of the optical modes within each resonator across the periodic structure of the metasurface makes the emission process less sensitive to the position of the quantum emitter. This removes reliance on the limiting high-precision alignment during the fabrication processes. Additionally, the electric and magnetic dipole modes provide broadband enhancement of emission, reducing the critical need for wavelength alignment between quantum emitter and metasurface modes [188].

The metasurface design can be fine-tuned through its geometry to introduce selective modification of the emission properties of the quantum emitter, including enhanced photon extraction for selected orientations of the quantum emitter dipole moment [185, 198, 199, 200]. Metasurfaces provide an indefinite number of degrees of freedom in their design, with Huang et al. demonstrating a monolithically integrated metalens above a diamond nitrogen vacancy (Fig. 7f), fully removing the need for a collection objective [190], and Liu et al. using metasurfaces to generate circularly polarised vortex beams (Fig. 7e) [189].

While electron beam lithography (EBL) is often used for metasurface fabrication, other methods for

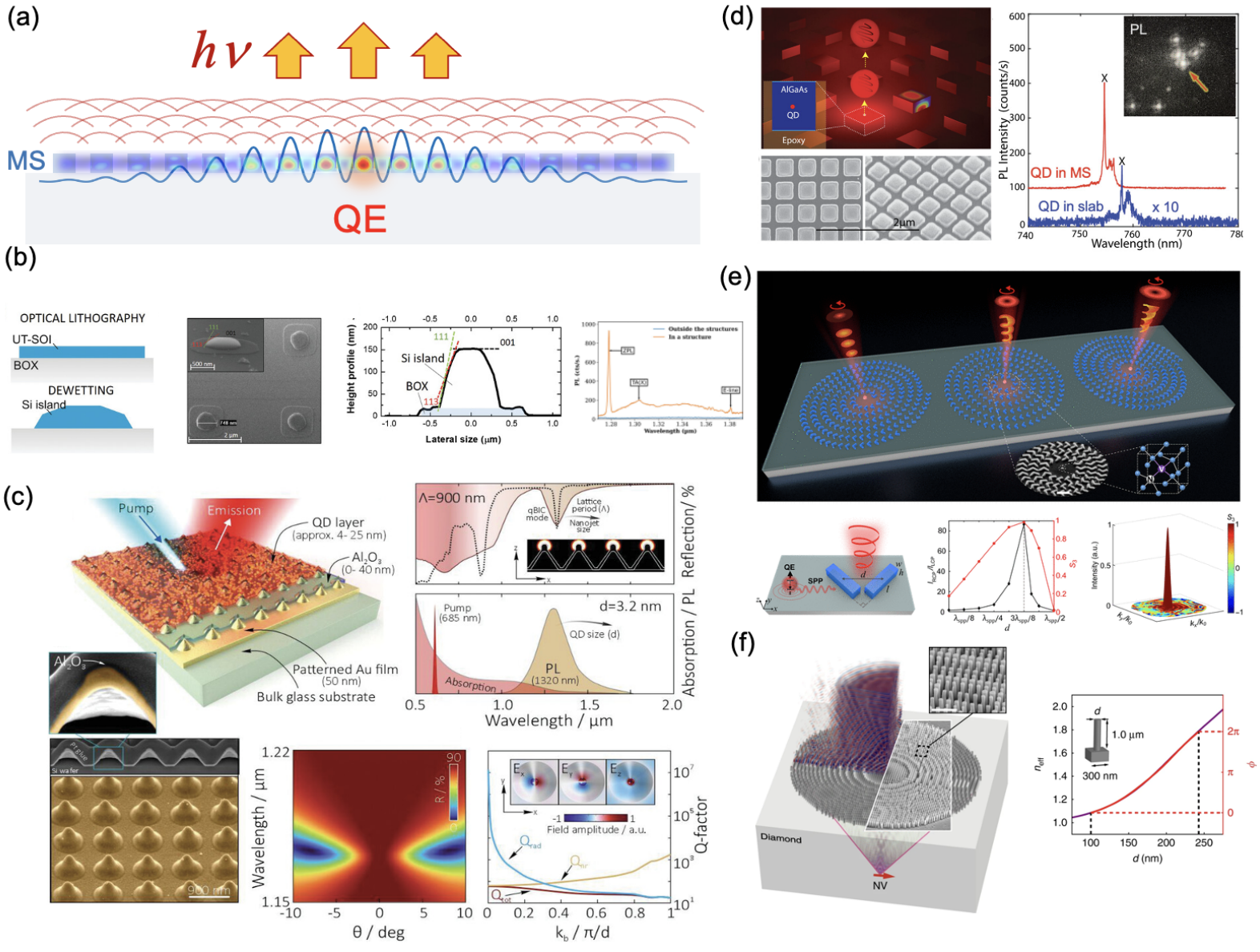


Figure 7: (a) Quantum emitter outcoupling through metasurface modes [185]. (b) Silicon colour centre coupling to a Mie resonance [186]. (c) Quantum dots coupling to bound states in the continuum provided by a plasmonic laser-printed metasurface [187]. (d) Huygens' Mie metasurface with an order of magnitude enhancement in observed emission brightness [188]. (e) Metasurfaces used for circularly polarised single photon beams [189]. (f) A flat metalens coupling to a diamond nitrogen vacancy, removing the requirement for a collection objective [190]. (a) Reprinted (adapted) from [185]. CC BY 4.0. (b) Reprinted (adapted) from [186]. CC BY 4.0. (c) From [187]. Reprinted (adapted) with permission from John Wiley and Sons. Copyright © 2023, John Wiley and Sons. (d) From [188]. Reprinted (adapted) with permission from American Chemical Society. Copyright © 2024, American Chemical Society. (e) From [189]. Reprinted (adapted) with permission from AAAS. Copyright © 2023, The American Association for the Advancement of Science. (f) Reprinted (adapted) from [190]. CC BY 4.0.

larger scale production have also been developed, such as nanoimprint lithography (NIL) [201]. Additionally, Sergeeva et al. have demonstrated laser-printed plasmonic metasurfaces coupled to quantum dots (Fig. 7c) [187]. As the collection efficiency of systems using these metasurfaces is significantly higher, lower pumping powers can be used, allowing the quantum emitters to operate in regimes with more desirable properties. [188].

These examples show how metasurfaces can be used to access properties of quantum light and how metasurfaces are providing increasing levels of enhancement and fabrication resilience, proving that they are becoming the ideal solution for enhancing the emission from quantum emitters. This rapid progress shows how this is just the tip of the iceberg of what we can achieve by combining metasurfaces and quantum emitters. Progress continues at a rapid pace, and the effects of this work will be significant in quantum photonics, where emission from these systems will be harnessed for powerful applications.

**Spontaneous parametric down-conversion from Metasurfaces**

Another way to generate single photons is via a quantum process called spontaneous parametric down-conversion (SPDC). In quantum optics, SPDC has been used for several applications such as quantum imaging, quantum key distribution, etc. The first direct demonstration of SPDC from a metasurface was achieved only until 2021 [202]. Since then, there has been remarkable progress in demonstrating in situ generation and engineering of SPDC from 'quantum optical' metasurfaces (QOMs). In fact, due to its delicate experimental implementation, the first applications of metasurfaces for SPDC focused on the manipulation of the emission rather than its generation [203, 204]. In this section, we focus on reviewing the different existing experimental works and we will provide a perspective at the end. It is important to mention that, because this field is at its infancy, all the existing works have focused on passive control so far.

As mentioned above, the first experiment that demonstrated the generation of photon pairs via SPDC from metasurfaces was performed using $LiNbO_3$ metasurfaces featuring resonances of Mie type [202]. The authors demonstrated a two orders of magnitude enhancement of frequency-degenerate emission of photon pairs when compared to an unpatterned $LiNbO_3$ film of the same thickness [Figure 8 (a, b)]. Because of the metasurface design, the photon pairs were emitted in backward direction, which was not seen before in SPDC. This metasurface design could not generate frequency-nondegenerate photon pairs with an efficiency higher than the unpatterned film. This work suggested one potential application of metasurfaces for SPDC: the control of the direction of emission.

To further exploit their capabilities, the next generation of metasurfaces for SPDC focused on the exploitation of a more general class of resonances, namely quasi-bound states in the continuum (qBIC) resonances [211]. In contrast to Mie-type resonances, qBICs feature higher quality factors, and thus higher conversion efficiencies are expected. T. Santiago-Cruz et al. fabricated GaAs metasurfaces featuring multiple qBICs in the near-infrared wavelength range [205]. The authors demonstrated, for the first time, multiplexed frequency-degenerate and non-degenerate photon pair emission driven by multiple qBICs over a large frequency range [Figure 8 (c, d)]. The multiple qBIC resonances are uncoupled and depending on the pump polarization, it is possible to choose which resonance-driven process to observe. The photon pairs exhibited a narrow spectrum given by the linewidth of the resonances. In this work, the photons were emitted in a forward direction. Remarkably, without the resonances it would be impossible to obtain a measurable signal. Indeed, the (001) crystallographic orientation of the GaAs wafer used in the fabrication is not optimal for emission in the normal direction. The authors estimated the enhancement to be at least three orders of magnitude. In a recent follow-up study, J. Noh et al analyzed the polarization properties of photon pairs emitted by these qBICs [212]. The authors concluded that the photon pairs inherit the polarization properties of the resonance modes driving the nonlinear interaction. This work demonstrates an interesting application: the generation of photon pairs with tailored polarization.

With the ideas of the last two works in mind, C. Son et al designed a qBIC-resonant GaP metasurface [Figure 8 (e, f)] and demonstrated bi-directional emission of frequency-nondegenerate photon pairs, with the resonant photon being emitted backwards, while its conjugate partner photon is emitted forwards [Figure 8 (g) middle panel], i. e., the authors were able to control the directions of emission and wavelengths of the photon pairs [206]. For any other detection configuration, forward-forward (left-hand panel in Figure 8 (g)]) and backward-backward (right-hand panel in Figure 8 (g)]), the authors did not observe any fingerprint of the resonant behavior. Here, the authors observed a moderate 67-fold enhancement with respect to an unpatterned GaP film of the same thickness and emitting photon pairs in the forward direction, which is its most efficient configuration given the film thickness.

The works we have reviewed so far are all based on semiconductor metasurfaces. Recently, W. Jia et al bridged the gap and reported the first observation of SPDC from a plasmonic metasurface [213]. The metasurface consists of an array of split-ring gold nanoresonators deposited on an ITO substrate. The metasurface was designed as a doubly-resonant system, that is, one resonance for the pump wavelength, and another for the SPDC wavelength. Since the thickness of the surface is very thin, the authors used the ITO layer to couple the resonance behavior of the nanoresonator array with the epsilon-near-zero mode of the ITO layer, which leads to a stronger second-order nonlinear response. In contrast to other QOMs, here

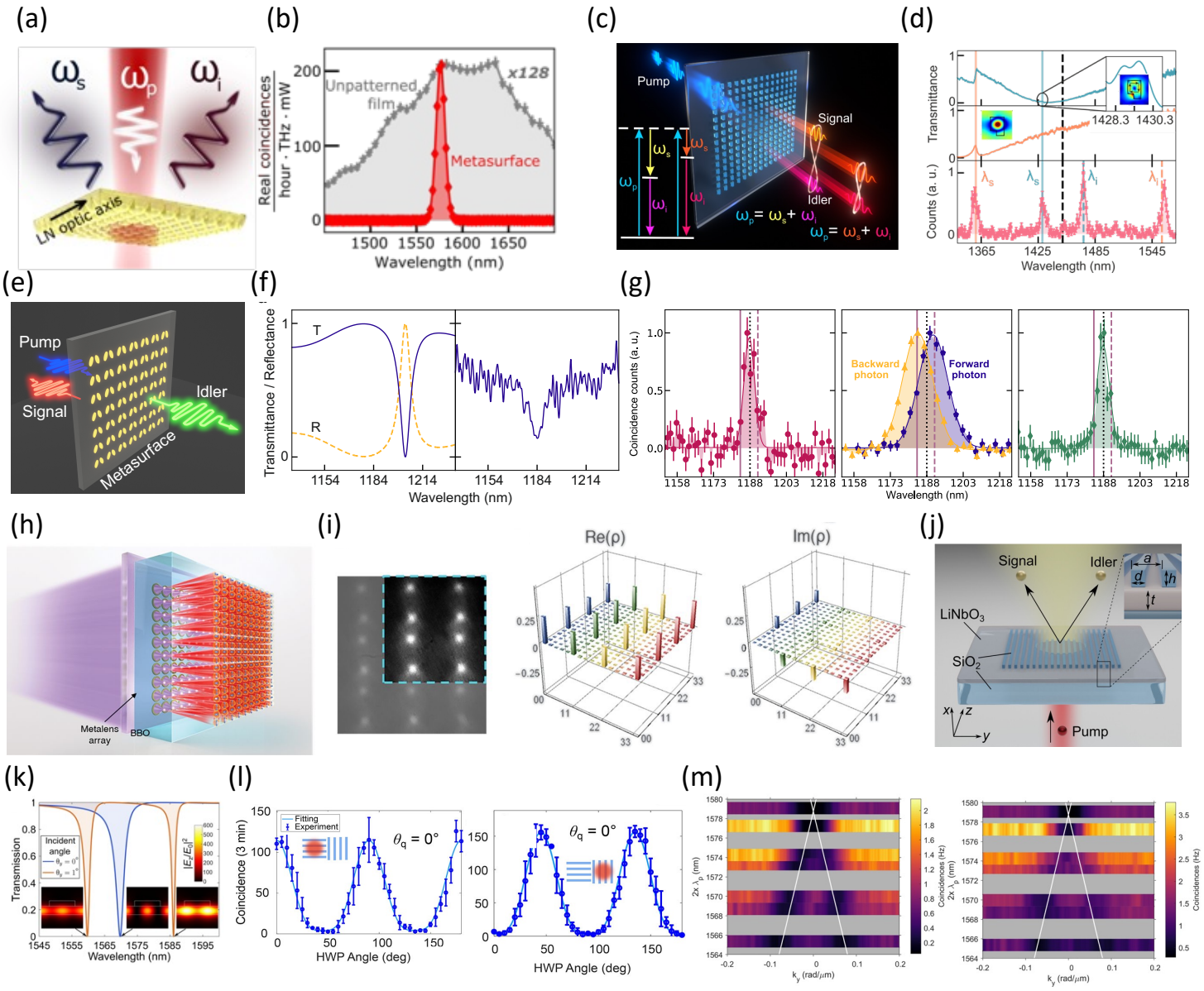


Figure 8: (a-b) Backward generation of frequency-degenerate photon pairs via SPDC in a $LiNbO_3$ metasurface featuring Mie-type resonances. The pair generation rate is enhanced by more than two orders of magnitude compared to an unpatterned $LiNbO_3$ film of the same thickness [202]. (c-d) Two qBICs independently generating frequency-multiplexed photon pairs in a GaAs metasurface. The electric dipole resonance at 1359.4 nm (central panel in (d)) generates a photon pair with the signal photon emitted at the resonance wavelength, while its conjugate idler photon is generated at the wavelength that conserves energy (bottom panel in (d)) given the pump laser wavelength. Likewise, a magnetic dipole resonance at 1429.4 nm (top panel in (d)) generates a another photon pair at different wavelengths under the same rules. [205]. (e-g) SPDC in a GaP metasurfaces featuring a qBIC resonance (left panel in (f): simulated reflection and transmission spectra. Right panel in (f): measured transmission spectrum). The resonant photon at 1184 nm is emitted backwards, while its conjugate partner photon is emitted forwards (middle panel in (g)). For any other detection configuration, i.e., forward-forward (left-hand panel in (g)) or backward-backward (right-hand panel in (g)), the SPDC spectrum shows photon pairs only within the spectral overlap of the forward-backward configuration (middle panel in (g)). [206]. (h-i) Multi-SPDC generation in a BBO crystal coupled to a metalens array. The metalens focuses the pump laser in an array of 10x10 spots inside the BBO crystal. Panel (i) shows the measured density matrix for a four-dimensional entangled state [207]. (j-m) Frequency-degenerate SPDC from a nonlocal metasurface. An $SiO_2$ metagrating supports nonlocal qBICs that enhance near fields inside a $LiNbO_3$ film (panel (k)). The in-plane orientation of the metagrating dictates the polarization of the emitted photon pairs (panel (l), the insets show the orientation of the metagrating). The angle of emission of frequency-degenerate photon pairs can be tuned via the pump wavelength $\lambda_p$ in both forward -forward (left-hand panel in (m)) and forward-backward (right-hand panel in (m)) directions of emission of the signal-idler pair [208, 209, 210]. (a-b) Reprinted (adapted) with permission from [202]. Copyright © 2021, American Chemical Society. (c-d) From [205]. Reprinted with permission from AAAS. Copyright © 2022, The American Association for the Advancement of Science. (e-g) Reproduced from Ref. [206] with permission from the Royal Society of Chemistry. (h-i) From [207]. Reprinted with permission from AAAS. Copyright © 2020, The American Association for the Advancement of Science. (j-k) From [208]. Reprinted with permission from AAAS. Copyright © 2022, The American Association for the Advancement of Science. (l) Reprinted (adapted) with permission from [209]. Copyright © 2023, American Chemical Society. (m) Adapted from [210]. CC BY 4.0.

the surface is the origin of the nonlinearity, as neither gold nor ITO possess intrinsic bulk second-order susceptibility. More precisely, the photon-pair generation occurs at the gold-ITO interface. In addition, the authors also tackled another open problem, namely the generation of polarization-entangled photon pairs from metasurfaces: by an appropriate choice of the pump polarization they demonstrated the generation of one of the Bell states.

In addition to the aforementioned works, there have been a series of studies utilizing metasurfaces to manipulate the generation of SPDC in the adjacent substrate. For instance, [207] fabricated a metalens array on a 0.5 mm-thick BBO crystal. The design consisted of 100 metalenses arranged in a 10 x 10 array that focused the pump laser into 100 spots in the BBO crystal [Figure 8 (h-i)]. In this way, the metalens array triggered the coherent generation of an array of 10x10 photon pairs.

In a similar manner, there is a collection of works [208, 209, 210, 214] based on an $SiO_2$ metagrating fabricated atop a $\sim$ 300 nm-thick $LiNbO_3$ film [Figure 8 (j)]. Here, the metagrating supports nonlocal qBICs that enhance the zero-point vacuum fluctuations inside the $LiNbO_3$ film, where the generation of SPDC occurs [Figure 8 (k)]. This platform is the most explored among all QOMs in terms of applications. In the first work, J. Zhang et al. demonstrated the generation of spatially-entangled photon pairs [208]. In the second work, J. Ma et al showed that the polarization state of the photon pairs is dictated mainly by the orientation of the grating rather than by the elements of the $\chi^{(2)}$ tensor [209], offering an option to control the polarization of the photons via the grating orientation [Figure 8 (l)]. In the subsequent work, M. A. Weissflog et al used this platform to demonstrate the control of the angle and direction (i.e., forward-forward or forward-backward) of emission of frequency-degenerate photon pairs [210]. The emission angle is controlled by the pump laser wavelength [Figure 8 (m)]. In the most recent work, J. Ma et al went a step forward and used the photon pairs generated in this platform in a ghost imaging application [214]. Certainly, this hybrid platform can potentially perform the multi-operation of controlling the angle of emission, the wavelength, and the polarization of the emitted photon pairs in a single device. One of the advantages of this platform is its large transparency window compared to those made of GaAs or GaP, which is crucial to minimize spurious incoherent emission such as photoluminescence. An open task in this platform is the generation of frequency-nondegenerate photon pairs.

In summary, QOMs are slowly finding their way in the quantum domain. There is, certainly, one important problem that must be addressed before any practical implementation. SPDC is a second-order nonlinear process and as such, long interaction lengths are needed to achieve large efficiencies. Because of the subwavelength thickness, SPDC from QOMs result in low conversion efficiencies. To date, the highest pair-generation rate reported is only 0.002 Hz/(mW·nm) [205]. Different pathways can be adopted to enhance the pair-generation rates: (i) design metasurfaces with higher quality (Q) factors. Currently, the Q factors that have been exploited are in the range of 10-$10^3$. There are metasurfaces designs that sustain Q factors in the order of $10^4$ [215]. For frequency-degenerate emission, this will result in a conversion efficiency enhanced by $10^2$. (ii) Use of materials with high second-order nonlinearity. In this regard, semiconductors such as GaAs, AlGaAs, and InGaP are very attractive as they possess one of the highest $\chi^{(2)}$ values. Moreover, their nanofabrication is more advanced than, for instance, $LiNbO_3$. (iii) In connection with the previous point, some materials may exhibit complex $\chi^{(2)}$ tensors, and the optimization of the overlap integral between the interacting modes (in the case of SPDC, the pump, signal and idler modes). So far, some of the aforementioned platforms [202, 206, 212], have not optimized this parameter. Such optimization involves an appropriate choice of crystallographic orientation of the nonlinear material, a careful selection of the resonance modes together with the in-plane orientation of the nanoresonators with respect to the crystallographic axes.

Finally, quantum third-order nonlinear optical effects such as third-order spontaneous parametric down-conversion, i. e., the direct decay of a pump photon into three daughter photons in a third-order ($\chi^{(3)}$) nonlinear medium, and spontaneous four-wave mixing (SFWM), i. e., the decay of two pump photons into two daughter photons in a $\chi^{(3)}$ nonlinear medium, are yet to be observed in QOMs. Meanwhile, J. Yang et al made a step toward by doing stimulated emission tomography of SFWM in plasmonic nanoantenas [216].

## Conclusion

In summary, we have highlighted recent advancements in using metasurfaces—structured 2D materials that control light-matter interactions at sub-wavelength scales—to manipulate spontaneous emission. Specifically, we review the impact of metasurfaces across three key emission types: thermal, luminescent, and quantum.

In the field of thermal emission, metasurfaces have unlocked new possibilities for controlling incoherent radiation by engineering the spatial, temporal, and spin coherence of emitted light. These innovations have direct implications for applications such as thermal energy management, passive radiative cooling, and thermophotonic devices. The ability to precisely sculpt thermal radiation not only enhances energy efficiency but also opens pathways for novel technologies like thermal camouflage and thermal imaging. As metasurfaces evolve, their role in advanced energy-harvesting systems and next-generation infrared sensing devices will likely expand.

For luminescent emission, metasurfaces have driven significant advancements in enhancing emission rates and improving light extraction efficiency, achieving wavefront control of emission, and actively redirecting emission patterns. These improvements are critical for optoelectronic devices such as LEDs and display systems, where efficient conversion of electrical energy to light is key. Metasurfaces have shown the potential to overcome longstanding challenges in lighting and display technologies, particularly in applications requiring high brightness and precise control over light directionality and polarization. The integration of metasurfaces into everyday devices—such as augmented reality displays, high-efficiency lighting, and next-generation sensors—signals a new era of energy-efficient and highly functional photonic systems.

In quantum emission, metasurfaces have shown extraordinary promise in advancing single-photon sources and manipulating quantum states. The ability to control quantum light emission at the level of individual photons is crucial for developing quantum communication, quantum computing, and sensing technologies. By facilitating on-demand, deterministic photon emission and supporting the manipulation of quantum states, metasurfaces are laying the groundwork for the future of quantum technologies, where secure communication and advanced computation methods will be paramount.

Looking ahead, the development of active metasurfaces capable of dynamic, real-time control over emission properties represents a promising frontier. Tremendous advancements have been made in using machine learning and inverse design algorithms to design and optimize metasurfaces.[217, 218] By leveraging AI-driven algorithms, researchers can rapidly explore large design spaces and optimize metasurface structures for specific performance criteria, significantly accelerating the discovery of novel metasurface designs and functionalities.[141, 219] As these technologies mature, metasurfaces will continue to expand their role in advancing optical systems and light-based applications across a wide range of industries. By providing fine-tuned control over light-matter interactions at the nanoscale, metasurfaces have redefined the boundaries of what is possible for incoherent light manipulation.

**Acknowledgements**

This work was supported by the U.S. Department of Energy, Office of Basic Energy Sciences, Division of Materials Sciences and Engineering and performed, in part, at the Center for Integrated Nanotechnologies, an Office of Science User Facility operated for the U.S. Department of Energy (DOE) Office of Science. Sandia National Laboratories is a multi-mission laboratory managed and operated by National Technology and Engineering Solutions of Sandia, LLC, a wholly owned subsidiary of Honeywell International, Inc., for the U.S. Department of Energy's National Nuclear Security Administration under contract DE-NA0003525. This paper describes objective technical results and analysis. Any subjective views or opinions that might be expressed in the paper do not necessarily represent the views of the U.S. Department of Energy or the United States Government. SB and ZJ would like to acknowledge the support from the U.S. Department of Energy (DOE), Office of Basic Sciences under DE-SC0017717. WM is supported by a U.S. Department of Defense (DOD) National Defense Science and Engineering Graduate (NDSEG) Fellowship. The work of WM and JS was supported by the Office of Naval Research (Grant #N00014–22–1–2337). SP is supported

by the EPSRC (EP/S022139/1).

## References


[1] A. G. Curto, G. Volpe, T. H. Taminiau, M. P. Kreuzer, R. Quidant, N. F. van Hulst, *Science* **2010**, *329*, 5994 930, publisher: American Association for the Advancement of Science.

[2] S. Liu, A. Vaskin, S. Addamane, B. Leung, M.-C. Tsai, Y. Yang, P. P. Vabishchevich, G. A. Keeler, G. Wang, X. He, Y. Kim, N. F. Hartmann, H. Htoon, S. K. Doorn, M. Zilk, T. Pertsch, G. Balakrishnan, M. B. Sinclair, I. Staude, I. Brener, *Nano Letters* **2018**, *18*, 11 6906, publisher: American Chemical Society.

[3] P. P. Iyer, R. A. DeCrescent, Y. Mohtashami, G. Lheureux, N. A. Butakov, A. Alhassan, C. Weisbuch, S. Nakamura, S. P. DenBaars, J. A. Schuller, *Nature Photonics* **2020**, *14*, 9 543.

[4] G. Kirchhoff, *Von Kirchhoff bis Planck: Theorie der Wärmestrahlung in Historisch-kritischer Darstellung* **1978**, 131–151.

[5] J. J. Sanchez-Mondragon, N. B. Narozhny, J. H. Eberly, *Phys. Rev. Lett.* **1983**, *51* 550.

[6] M. Kira, F. Jahnke, W. Hoyer, S. Koch, *Progress in Quantum Electronics* **1999**, *23*, 6 189.

[7] D. Klyshko, *Photons Nonlinear Optics*, CRC Press, **2018**.

[8] C. Okoth, A. Cavanna, T. Santiago-Cruz, M. V. Chekhova, *Phys. Rev. Lett.* **2019**, *123* 263602.

[9] T. Santiago-Cruz, V. Sultanov, H. Zhang, L. A. Krivitsky, M. V. Chekhova, *Opt. Lett.* **2021**, *46*, 3 653.

[10] C. Okoth, E. Kovlakov, F. Bönsel, A. Cavanna, S. Straupe, S. P. Kulik, M. V. Chekhova, *Phys. Rev. A* **2020**, *101* 011801.

[11] S. Bai, C. Liu, *Renewable and Sustainable Energy Reviews* **2021**, *147* 111188.

[12] O. Ilic, P. Bermel, G. Chen, J. D. Joannopoulos, I. Celanovic, M. Soljačić, *Nature nanotechnology* **2016**, *11*, 4 320.

[13] D. G. Baranov, Y. Xiao, I. A. Nechepurenko, A. Krasnok, A. Alù, M. A. Kats, *Nature materials* **2019**, *18*, 9 920.

[14] A. P. Raman, M. A. Anoma, L. Zhu, E. Rephaeli, S. Fan, *Nature* **2014**, *515*, 7528 540.

[15] A. Lochbaum, Y. Fedoryshyn, A. Dorodnyy, U. Koch, C. Hafner, J. Leuthold, *ACS photonics* **2017**, *4*, 6 1371.

[16] C. Guo, B. Zhao, S. Fan, *Physical Review X* **2022**, *12*, 2 021023.

[17] S. Bharadwaj, Z. Jacob, *Science* **2024**, *386*, 6728 1348.

[18] T. Liu, C. Guo, W. Li, S. Fan, *ELight* **2022**, *2*, 1 25.

[19] Q. Chu, F. Zhong, X. Shang, Y. Zhang, S. Zhu, H. Liu, *Nanophotonics* **2024**, *13*, 8 1279.

[20] M. F. Picardi, K. N. Nimje, G. T. Papadakis, *Journal of Applied Physics* **2023**, *133*, 11.

[21] J. E. Vázquez-Lozano, I. Liberal, *ACS Applied Optical Materials* **2024**, *2*, 6 898.

[22] X. Wang, Z. Jacob, *Light: Science & Applications* **2022**, *11*, 1 342.

[23] K. J. Shayegan, S. Biswas, B. Zhao, S. Fan, H. A. Atwater, *Nature Photonics* **2023**, *17*, 10 891.

[24] M. Zhou, E. Khoram, D. Liu, B. Liu, S. Fan, M. L. Povinelli, Z. Yu, *ACS Photonics* **2021**, *8*, 2 497.

[25] W. Li, S. Fan, *Optics express* **2018**, *26*, 12 15995.

[26] J. Yu, R. Qin, Y. Ying, M. Qiu, Q. Li, *Advanced Materials* **2023**, *35*, 45 2302478.

[27] X. Wang, T. Sentz, S. Bharadwaj, S. K. Ray, Y. Wang, D. Jiao, L. Qi, Z. Jacob, *Science Advances* **2023**, *9*, 4 eade4203.

[28] J.-J. Greffet, R. Carminati, K. Joulain, J.-P. Mulet, S. Mainguy, Y. Chen, *Nature* **2002**, *416*, 6876 61.

[29] J. H. Park, S. E. Han, P. Nagpal, D. J. Norris, *ACS Photonics* **2016**, *3*, 3 494.

[30] Y. C. Jun, T. S. Luk, A. Robert Ellis, J. F. Klem, I. Brener, *Applied Physics Letters* **2014**, *105*, 13.

[31] P. P. Iyer, M. Pendharkar, C. J. Palmstrøm, J. A. Schuller, *Nature communications* **2017**, *8*, 1 472.

[32] I. Liberal, N. Engheta, *Proceedings of the National Academy of Sciences* **2018**, *115*, 12 2878.

[33] S. Molesky, C. J. Dewalt, Z. Jacob, *Optics express* **2013**, *21*, 101 A96.

[34] S. Pendharker, H. Hu, S. Molesky, R. Starko-Bowes, Z. Poursoti, S. Pramanik, N. Nazemifard, R. Fedosejevs, T. Thundat, Z. Jacob, *Journal of Optics* **2017**, *19*, 5 055101.

[35] J. Xu, J. Mandal, A. P. Raman, *Science* **2021**, *372*, 6540 393.

[36] Y. Ying, B. Ma, J. Yu, Y. Huang, P. Ghosh, W. Shen, M. Qiu, Q. Li, *Laser & Photonics Reviews* **2022**, *16*, 8 2200018.

[37] P. N. Dyachenko, S. Molesky, A. Y. Petrov, M. Störmer, T. Krekeler, S. Lang, M. Ritter, Z. Jacob, M. Eich, *Nature communications* **2016**, *7*, 1 11809.

[38] X. Liu, T. Tyler, T. Starr, A. F. Starr, N. M. Jokerst, W. J. Padilla, *Physical review letters* **2011**, *107*, 4 045901.

[39] M. De Zoysa, T. Asano, K. Mochizuki, A. Oskooi, T. Inoue, S. Noda, *Nature Photonics* **2012**, *6*, 8 535.

[40] T. Asano, M. Suemitsu, K. Hashimoto, M. De Zoysa, T. Shibahara, T. Tsutsumi, S. Noda, *Science advances* **2016**, *2*, 12 e1600499.

[41] S. Yu, P. Zhou, W. Xi, Z. Chen, Y. Deng, X. Luo, W. Li, J. Shiomi, R. Hu, *Light: Science & Applications* **2023**, *12*, 1 291.

[42] F. P. Lanter, A. Sutinjo, J. Morgan, *Advances in Space Research* **2023**, *72*, 12 5503.

[43] A. Basiri, X. Chen, J. Bai, P. Amrollahi, J. Carpenter, Z. Holman, C. Wang, Y. Yao, *Light: Science & Applications* **2019**, *8*, 1 78.

[44] K. P. Gurton, A. J. Yuffa, G. W. Videen, *Optics letters* **2014**, *39*, 13 3857.

[45] J. A. Schuller, T. Taubner, M. L. Brongersma, *Nature Photonics* **2009**, *3*, 11 658.

[46] J. Mason, S. Smith, D. Wasserman, *Applied Physics Letters* **2011**, *98*, 24.

[47] J. Angel, J. Landstreet, *Astrophysical Journal, vol. 178, p. L21* **1972**, *178* L21.

[48] S. De, H. Tashiro, *Physical Review D* **2015**, *92*, 12 123506.

[49] J. Bailey, A. Chrysostomou, J. Hough, T. Gledhill, A. McCall, S. Clark, F. Ménard, M. Tamura, *Science* **1998**, *281*, 5377 672.

[50] W. Sparks, J. H. Hough, T. A. Germer, F. Robb, L. Kolokolova, *Planetary and Space Science* **2012**, *72*, 1 111.

[51] M. Roknuzzaman, S. Bharadwaj, Y. Wang, C. Khandekar, D. Jiao, R. Rahman, Z. Jacob, *Physical Review B* **2023**, *108*, 22 224307.

[52] H. Wang, H. Wu, Z. Shen, *Optics Express* **2017**, *25*, 16 19609.

[53] A. Ott, P. Ben-Abdallah, S.-A. Biehs, *Physical Review B* **2018**, *97*, 20 205414.

[54] Y. Wang, C. Khandekar, X. Gao, T. Li, D. Jiao, Z. Jacob, *Optical Materials Express* **2021**, *11*, 11 3880.

[55] B. Zhao, C. Guo, C. A. Garcia, P. Narang, S. Fan, *Nano letters* **2020**, *20*, 3 1923.

[56] C. Yang, W. Cai, Z. M. Zhang, *Phys. Rev. B* **2022**, *106* 245407.

[57] E. Khan, E. E. Narimanov, *Physical Review B* **2019**, *100*, 8 081408.

[58] N. Shitrit, I. Yulevich, E. Maguid, D. Ozeri, D. Veksler, V. Kleiner, E. Hasman, *Science* **2013**, *340*, 6133 724.

[59] C. Khandekar, Z. Jacob, *Phys. Rev. Appl.* **2019**, *12* 014053.

[60] S. C. Malek, A. C. Overvig, S. Shrestha, N. Yu, *Nanophotonics* **2020**, *10*, 1 655.

[61] A. C. Overvig, S. A. Mann, A. Alù, *Physical Review X* **2021**, *11*, 2 021050.

[62] J. R. Nolen, A. C. Overvig, M. Cotrufo, A. Alù, *Nature Nanotechnology* **2024**, 1–8.

[63] J. R. Nolen, A. C. Overvig, M. Cotrufo, A. Alù, *Nature Nanotechnology* **2024**, 1–8.

[64] J. von Neumann, E. P. Wigner, *The Collected Works of Eugene Paul Wigner: Part A: The Scientific Papers* **1993**, 291–293.

[65] B. Zhen, C. W. Hsu, L. Lu, A. D. Stone, M. Soljačić, *Physical review letters* **2014**, *113*, 25 257401.

[66] F. Bao, S. Jape, A. Schramka, J. Wang, T. E. McGraw, Z. Jacob, *Optics Express* **2024**, *32*, 3 3852.

[67] F. Bao, X. Wang, S. H. Sureshbabu, G. Sreekumar, L. Yang, V. Aggarwal, V. N. Boddeti, Z. Jacob, *Nature* **2023**, *619*, 7971 743.

[68] X. Wang, Z. Yang, F. Bao, T. Sentz, Z. Jacob, *Optica* **2024**, *11*, 1 73.

[69] X. Wang, T. Van Mechelen, S. Bharadwaj, M. Roknuzzaman, F. Bao, R. Rahman, Z. Jacob, *eLight* **2024**, *4*, 1 1.

[70] Y. Zhai, Y. Ma, S. N. David, D. Zhao, R. Lou, G. Tan, R. Yang, X. Yin, *Science* **2017**, *355*, 6329 1062.

[71] D. Li, X. Liu, W. Li, Z. Lin, B. Zhu, Z. Li, J. Li, B. Li, S. Fan, J. Xie, et al., *Nature Nanotechnology* **2021**, *16*, 2 153.

[72] K. Lin, S. Chen, Y. Zeng, T. C. Ho, Y. Zhu, X. Wang, F. Liu, B. Huang, C. Y.-H. Chao, Z. Wang, et al., *Science* **2023**, *382*, 6671 691.

[73] S. Zeng, S. Pian, M. Su, Z. Wang, M. Wu, X. Liu, M. Chen, Y. Xiang, J. Wu, M. Zhang, et al., *Science* **2021**, *373*, 6555 692.

[74] E. M. Purcell, In *Confined Electrons and Photons: New Physics and Applications*, 839–839. Springer, **1995**.

[75] W.-J. Joo, J. Kyoung, M. Esfandyarpour, S.-H. Lee, H. Koo, S. Song, Y.-N. Kwon, S. H. Song, J. C. Bae, A. Jo, M.-J. Kwon, S. H. Han, S.-H. Kim, S. Hwang, M. L. Brongersma, *Science* **2020**, *370*, 6515 459, publisher: American Association for the Advancement of Science.

[76] C. Würth, P. Manley, R. Voigt, D. Ahiboz, C. Becker, U. Resch-Genger, *Nano Letters* **2020**, *20*, 9 6682, publisher: American Chemical Society.

[77] I. Kim, R. J. Martins, J. Jang, T. Badloe, S. Khadir, H.-Y. Jung, H. Kim, J. Kim, P. Genevet, J. Rho, *Nature Nanotechnology* **2021**, *16*, 5 508, publisher: Nature Publishing Group.

[78] S. Cao, Y. Jin, H. Dong, T. Guo, J. He, S. He, *Journal of Physics: Materials* **2021**, *4*, 3 035001, publisher: IOP Publishing.

[79] M. Wang, F. Xu, Y. Lin, B. Cao, L. Chen, C. Wang, J. Wang, K. Xu, *Nanoscale* **2017**, *9*, 26 9104, publisher: The Royal Society of Chemistry.

[80] T.-Y. Huang, R. R. Grote, S. A. Mann, D. A. Hopper, A. L. Exarhos, G. G. Lopez, A. R. Klein, E. C. Garnett, L. C. Bassett, *Nature Communications* **2019**, *10*, 1 2392, publisher: Nature Publishing Group.

[81] E. Khaidarov, Z. Liu, R. Paniagua-Domínguez, S. T. Ha, V. Valuckas, X. Liang, Y. Akimov, P. Bai, C. E. Png, H. V. Demir, A. I. Kuznetsov, *Laser & Photonics Reviews* **2020**, *14*, 1 1900235, _eprint: https://onlinelibrary.wiley.com/doi/pdf/10.1002/lpor.201900235.

[82] J. Huang, Z. Hu, X. Gao, Y. Xu, L. Wang, *Optics Letters* **2021**, *46*, 14 3476, publisher: Optica Publishing Group.

[83] P. Mao, C. Liu, X. Li, M. Liu, Q. Chen, M. Han, S. A. Maier, E. H. Sargent, S. Zhang, *Light: Science & Applications* **2021**, *10*, 1 180, publisher: Nature Publishing Group.

[84] J.-Q. Wang, Z.-W. Qin, Y.-L. Ma, Y. Yang, H.-Y. Huang, C.-S. Guo, Q.-Y. Yue, *Optics Communications* **2023**, *532* 129251.

[85] M. S. Abdelkhalik, A. Vaskin, T. López, A. M. Berghuis, A. Abass, J. G. Rivas, *Nanophotonics* **2023**, *12*, 18 3553, publisher: De Gruyter.

[86] S. Park, D. Kim, Y.-S. Choi, A. Baucour, D. Kim, S. Yoon, K. Watanabe, T. Taniguchi, J. Shin, J. Kim, M.-K. Seo, *Nano Letters* **2023**, *23*, 6 2158, pMID: 36854053.

[87] P. Törmä, W. L. Barnes, *Reports on Progress in Physics* **2014**, *78*, 1 013901, publisher: IOP Publishing.

[88] L. Novotny, N. van Hulst, *Nature Photonics* **2011**, *5*, 2 83, publisher: Nature Publishing Group.

[89] S. Wu, H. Xia, J. Xu, X. Sun, X. Liu, *Advanced Materials* **2018**, *30*, 47 1803362, _eprint: https://onlinelibrary.wiley.com/doi/pdf/10.1002/adma.201803362.

[90] P. Anger, P. Bharadwaj, L. Novotny, *Physical Review Letters* **2006**, *96*, 11 113002, publisher: American Physical Society.

[91] G. Lozano, G. Grzela, M. A. Verschuuren, M. Ramezani, J. G. Rivas, *Nanoscale* **2014**, *6*, 15 9223, publisher: The Royal Society of Chemistry.

[92] R. Guo, S. Derom, A. I. Väkeväinen, R. J. A. v. Dijk-Moes, P. Liljeroth, D. Vanmaekelbergh, P. Törmä, *Optics Express* **2015**, *23*, 22 28206, publisher: Optica Publishing Group.

[93] S. Luo, Q. Li, Y. Yang, X. Chen, W. Wang, Y. Qu, M. Qiu, *Laser & Photonics Reviews* **2017**, *11*, 3 1600299.

[94] J. Cambiasso, G. Grinblat, Y. Li, A. Rakovich, E. Cortés, S. A. Maier, *Nano Letters* **2017**, *17*, 2 1219, publisher: American Chemical Society.

[95] C. Vidal, B. Tilmann, S. Tiwari, T. V. Raziman, S. A. Maier, J. Wenger, R. Sapienza, *Nano Letters* **2024**, *24*, 8 2437, publisher: American Chemical Society.

[96] K. Okamoto, I. Niki, A. Shvartser, Y. Narukawa, T. Mukai, A. Scherer, *Nature materials* **2004**, *3*, 9 601.

[97] G. Lozano, S. R. Rodriguez, M. A. Verschuuren, J. Gómez Rivas, *Light: Science & Applications* **2016**, *5*, 6 e16080.

[98] A. David, H. Benisty, C. Weisbuch, *Reports on Progress in Physics* **2012**, *75*, 12 126501.

[99] S. Wu, H. Xia, J. Xu, X. Sun, X. Liu, *Advanced Materials* **2018**, *30*, 47 1803362.

[100] S. Liu, A. Vaskin, S. Addamane, B. Leung, M.-C. Tsai, Y. Yang, P. P. Vabishchevich, G. A. Keeler, G. Wang, X. He, et al., *Nano letters* **2018**, *18*, 11 6906.

[101] H. Alhalaby, H. Zaraket, M. Principe, *Results in Optics* **2021**, *3* 100073.

[102] I. Staude, V. V. Khardikov, N. T. Fofang, S. Liu, M. Decker, D. N. Neshev, T. S. Luk, I. Brener, Y. S. Kivshar, *ACS Photonics* **2015**, *2*, 2 172, publisher: American Chemical Society.

[103] C. Zhang, Y. Xu, J. Liu, J. Li, J. Xiang, H. Li, J. Li, Q. Dai, S. Lan, A. E. Miroshnichenko, *Nature Communications* **2018**, *9*, 1 2964, publisher: Nature Publishing Group.

[104] A. Vaskin, S. Mashhadi, M. Steinert, K. E. Chong, D. Keene, S. Nanz, A. Abass, E. Rusak, D.-Y. Choi, I. Fernandez-Corbaton, T. Pertsch, C. Rockstuhl, M. A. Noginov, Y. S. Kivshar, D. N. Neshev, N. Noginova, I. Staude, *Nano Letters* **2019**, *19*, 2 1015, publisher: American Chemical Society.

[105] H. Sugimoto, M. Fujii, *ACS Photonics* **2021**, *8*, 6 1794, publisher: American Chemical Society.

[106] Z. Feng, T. Shi, G. Geng, J. Li, Z.-L. Deng, Y. Kivshar, X. Li, *eLight* **2023**, *3*, 1 21.

[107] Y. Gao, L. Liu, S. Murai, K. Shinozaki, K. Tanaka, *ACS Applied Materials & Interfaces* **2023**, *15*, 39 45960, publisher: American Chemical Society.

[108] A. F. Cihan, A. G. Curto, S. Raza, P. G. Kik, M. L. Brongersma, *Nature Photonics* **2018**, *12*, 5 284, publisher: Nature Publishing Group.

[109] L. Sun, C.-Y. Wang, A. Krasnok, J. Choi, J. Shi, J. S. Gomez-Diaz, A. Zepeda, S. Gwo, C.-K. Shih, A. Alù, X. Li, *Nature Photonics* **2019**, *13*, 3 180, publisher: Nature Publishing Group.

[110] Y. Liu, S. C. Lau, W.-H. Cheng, A. Johnson, Q. Li, E. Simmerman, O. Karni, J. Hu, F. Liu, M. L. Brongersma, T. F. Heinz, J. A. Dionne, *Nano Letters* **2023**, *23*, 13 6124, publisher: American Chemical Society.

[111] J. M. Richter, M. Abdi-Jalebi, A. Sadhanala, M. Tabachnyk, J. P. H. Rivett, L. M. Pazos-Outón, K. C. Gödel, M. Price, F. Deschler, R. H. Friend, *Nature Communications* **2016**, *7*, 1 13941, publisher: Nature Publishing Group.

[112] B. Gholipour, G. Adamo, D. Cortecchia, H. N. S. Krishnamoorthy, M. D. Birowosuto, N. I. Zheludev, C. Soci, *Advanced Materials* **2017**, *29*, 9 1604268, _eprint: https://onlinelibrary.wiley.com/doi/pdf/10.1002/adma.201604268.

[113] M. Klein, Y. Wang, J. Tian, S. T. Ha, R. Paniagua-Domínguez, A. I. Kuznetsov, G. Adamo, C. Soci, *Advanced Materials* **2022**.

[114] L. A. Muscarella, A. Cordaro, G. Krause, D. Pal, G. Grimaldi, L. S. D. Antony, D. Langhorst, A. Callies, B. Bläsi, O. Höhn, A. F. Koenderink, A. Polman, B. Ehrler, *ACS Applied Materials & Interfaces* **2022**, *14*, 33 38067, publisher: American Chemical Society.

[115] A. Y. Zhizhchenko, P. Tonkaev, D. Gets, A. Larin, D. Zuev, S. Starikov, E. V. Pustovalov, A. M. Zakharenko, S. A. Kulinich, S. Juodkazis, A. A. Kuchmizhak, S. V. Makarov, *Small* **2020**, *16*, 19 2000410, _eprint: https://onlinelibrary.wiley.com/doi/pdf/10.1002/smll.202000410.

[116] A. Kessel, C. Frydendahl, S. R. K. C. Indukuri, N. Mazurski, P. Arora, U. Levy, *Advanced Optical Materials* **2020**, *8*, 23 2001627, _eprint: https://onlinelibrary.wiley.com/doi/pdf/10.1002/adom.202001627.

[117] O. Aftenieva, J. Brunner, M. Adnan, S. Sarkar, A. Fery, Y. Vaynzof, T. A. F. König, *ACS Nano* **2023**, *17*, 3 2399, publisher: American Chemical Society.

[118] G. Xie, Z. Zhang, Q. Xue, S. Zhang, L. Zhao, Y. Luo, P. Chen, B. Quan, Y. Zhao, S. Liu, *Organic Electronics* **2010**, *11*, 12 2055.

[119] W. Song, X. Liang, S. Li, D. Li, R. Paniagua-Domínguez, K. H. Lai, Q. Lin, Y. Zheng, A. I. Kuznetsov, *Laser & Photonics Reviews* **2021**, *15*, 9 2000538.

[120] G. M. Akselrod, P. P. Iyer, R. D. Uthoff, Lidar systems based on tunable optical metasurfaces, **2021**, US Patent 11,092,675.

[121] E. Bailly, J.-P. Hugonin, J.-R. Coudevylle, C. Dabard, S. Ithurria, B. Vest, J.-J. Greffet, *ACS Nano* **2024**, *18*, 6 4903, publisher: American Chemical Society.

[122] L. Liu, F. Zhang, S. Murai, K. Tanaka, *Advanced Photonics Research* **2022**, *3*, 3 2100235, _eprint: https://onlinelibrary.wiley.com/doi/pdf/10.1002/adpr.202100235.

[123] M. Iwanaga, X. Yang, V. Karanikolas, T. Kuroda, Y. Sakuma, *Nanophotonics* **2024**, *13*, 1 95, publisher: De Gruyter.

[124] H. Hasebe, H. Sugimoto, T. Hinamoto, M. Fujii, *Advanced Optical Materials* **2020**, *8*, 22 2001148, _eprint: https://onlinelibrary.wiley.com/doi/pdf/10.1002/adom.202001148.

[125] S. Murai, G. W. Castellanos, T. V. Raziman, A. G. Curto, J. G. Rivas, *Advanced Optical Materials* **2020**, *8*, 16 1902024, _eprint: https://onlinelibrary.wiley.com/doi/pdf/10.1002/adom.201902024.

[126] N. Muhammad, Y. Chen, C.-W. Qiu, G. P. Wang, *Nano Letters* **2021**, *21*, 2 967, publisher: American Chemical Society.

[127] T. Wen, W. Zhang, S. Liu, A. Hu, J. Zhao, Y. Ye, Y. Chen, C.-W. Qiu, Q. Gong, G. Lu, *Science Advances* **2020**, *6*, 21 eaao0019, publisher: American Association for the Advancement of Science.

[128] A. Bashiri, A. Vaskin, K. Tanaka, M. Steinert, T. Pertsch, I. Staude, *ACS Nano* **2024**, *18*, 1 506, publisher: American Chemical Society.

[129] T. H. Taminiau, F. D. Stefani, N. F. v. Hulst, *Optics Express* **2008**, *16*, 14 10858, publisher: Optica Publishing Group.

[130] T. Coenen, E. J. R. Vesseur, A. Polman, A. F. Koenderink, *Nano Letters* **2011**, *11*, 9 3779, publisher: American Chemical Society.

[131] P. P. Iyer, R. A. DeCrescent, Y. Mohtashami, G. Lheureux, N. A. Butakov, A. Alhassan, C. Weisbuch, S. Nakamura, S. P. DenBaars, J. A. Schuller, *Nature Photonics* **2020**, *14*, 9 543, number: 9 Publisher: Nature Publishing Group.

[132] Y. Mohtashami, R. A. DeCrescent, L. K. Heki, P. P. Iyer, N. A. Butakov, M. S. Wong, A. Alhassan, W. J. Mitchell, S. Nakamura, S. P. DenBaars, J. A. Schuller, *Nature Communications* **2021**, *12*, 1 3591, number: 1 Publisher: Nature Publishing Group.

[133] K. Rong, B. Wang, A. Reuven, E. Maguid, B. Cohn, V. Kleiner, S. Katznelson, E. Koren, E. Hasman, *Nature Nanotechnology* **2020**, *15*, 11 927, publisher: Nature Publishing Group.

[134] J. Tian, G. Adamo, H. Liu, M. Klein, S. Han, H. Liu, C. Soci, *Advanced Materials* **2022**, *34*, 12 2109157, _eprint: https://onlinelibrary.wiley.com/doi/pdf/10.1002/adma.202109157.

[135] S. Hang, C.-M. Chuang, Y. Zhang, C. Chu, K. Tian, Q. Zheng, T. Wu, Z. Liu, Z.-H. Zhang, Q. Li, H.-C. Kuo, *Journal of Physics D: Applied Physics* **2021**, *54*, 15 153002, publisher: IOP Publishing.

[136] Y. Mohtashami, L. K. Heki, M. S. Wong, J. M. Smith, J. J. Ewing, W. J. Mitchell, S. Nakamura, S. P. DenBaars, J. A. Schuller, *Nano Letters* **2023**, *23*, 22 10505, publisher: American Chemical Society.

[137] M. Jeong, B. Ko, C. Jung, J. Kim, J. Jang, J. Mun, J. Lee, S. Yun, S. Kim, J. Rho, *Nano Letters* **2024**, *24*, 19 5783, publisher: American Chemical Society.

[138] P. P. Iyer, N. Karl, S. Addamane, S. D. Gennaro, M. B. Sinclair, I. Brener, *Nature Photonics* **2023**, *17*, 7 588.

[139] P. P. Iyer, S. Desai, S. Addamane, R. Dingreville, I. Brener, In *Proceedings of the IEEE/CVF Winter Conference on Applications of Computer Vision (WACV)*. **2023** 3770–3777.

[140] D. P. Kingma, *arXiv preprint arXiv:1312.6114* **2013**.

[141] S. Desai, S. Addamane, J. Y. Tsao, I. Brener, R. Dingreville, P. P. Iyer, Self-driving lab discovers principles for steering spontaneous emission, **2024**, URL `https://arxiv.org/abs/2407.16083`.

[142] R. K. Lee, Y. Xu, A. Yariv, *JOSA B* **2000**, *17*, 8 1438, publisher: Optica Publishing Group.

[143] A. F. Koenderink, M. Kafesaki, C. M. Soukoulis, V. Sandoghdar, *JOSA B* **2006**, *23*, 6 1196, publisher: Optica Publishing Group.

[144] S. Zhang, E. R. Martins, A. G. Diyaf, J. I. B. Wilson, G. A. Turnbull, I. D. W. Samuel, *Synthetic Metals* **2015**, *205* 127.

[145] X. Wang, Y. Li, R. Toufanian, L. C. Kogos, A. M. Dennis, R. Paiella, *Advanced Optical Materials* **2020**, *8*, 8 1901951, _eprint: https://onlinelibrary.wiley.com/doi/pdf/10.1002/adom.201901951.

[146] L. Heki, Y. Mohtashami, R. A. DeCrescent, A. Alhassan, S. Nakamura, S. P. DenBaars, J. A. Schuller, *ACS Omega* **2022**, *7*, 26 22477, publisher: American Chemical Society.

[147] L. K. Heki, Y. Mohtashami, R. Chao, J. J. Ewing, A. Quevedo, S. Nakamura, S. P. DenBaars, J. A. Schuller, *Advanced Optical Materials* **2024**, *12*, 16 2303186, _eprint: https://onlinelibrary.wiley.com/doi/pdf/10.1002/adom.202303186.

[148] Z. Li, P. Lin, Y.-W. Huang, J.-S. Park, W. T. Chen, Z. Shi, C.-W. Qiu, J.-X. Cheng, F. Capasso, *Science Advances* **2021**, *7*, 5 eabe4458, publisher: American Association for the Advancement of Science.

[149] Y. Mohtashami, L. K. Heki, A. Alhassan, S. Nakamura, S. P. DenBaars, J. A. Schuller, In *Conference on Lasers and Electro-Optics*. Optica Publishing Group, **2021** FM3K.2.

[150] Z. Zhuang, D. Iida, P. Kirilenko, K. Ohkawa, *Optics Express* **2021**, *29*, 19 29780, publisher: Optica Publishing Group.

[151] B. Krause, M. T. Pham, H. M. Luong, T. D. Nguyen, T. B. Hoang, *ACS Applied Nano Materials* **2022**, *5*, 1 1185, publisher: American Chemical Society.

[152] S. Iadanza, A. A. Liles, S. M. Butler, S. P. Hegarty, L. O'Faolain, *Optical Materials Express* **2021**, *11*, 9 3245, publisher: Optica Publishing Group.

[153] M. Keil, A. Emmanuel Wetzel, K. Wu, E. Khomtchenko, J. Urbankova, A. Boisen, T. Rindzevicius, A.-I. Bunea, R. J. Taboryski, *Nanoscale Advances* **2021**, *3*, 8 2236, publisher: Royal Society of Chemistry.

[154] P. Manley, M. Segantini, D. Ahiboz, M. Hammerschmidt, G. Arnaoutakis, R. W. MacQueen, S. Burger, C. Becker, *APL Photonics* **2021**, *6*, 3 036103.

[155] S. Murai, K. Agata, K. Tanaka, *Journal of Applied Physics* **2021**, *129*, 18 183101.

[156] C. Couteau, S. Barz, T. Durt, T. Gerrits, J. Huwer, R. Prevedel, J. Rarity, A. Shields, G. Weihs, *Nature Reviews Physics* **2023**, *5*, 6 354.

[157] A. J. Shields, *Nature photonics* **2007**, *1*, 4 215.

[158] T. Heindel, J.-H. Kim, N. Gregersen, A. Rastelli, S. Reitzenstein, *Advances in Optics and Photonics* **2023**, *15*, 3 613.

[159] C.-Y. Lu, J.-W. Pan, *Nature Nanotechnology* **2021**, *16*, 12 1294.

[160] J. Yang, Y. Chen, Z. Rao, Z. Zheng, C. Song, Y. Chen, K. Xiong, P. Chen, C. Zhang, W. Wu, et al., *Light: Science & Applications* **2024**, *13*, 1 33.

[161] J. Q. Grim, A. S. Bracker, M. Zalalutdinov, S. G. Carter, A. C. Kozen, M. Kim, C. S. Kim, J. T. Mlack, M. Yakes, B. Lee, et al., *Nature materials* **2019**, *18*, 9 963.

[162] R. Uppu, F. T. Pedersen, Y. Wang, C. T. Olesen, C. Papon, X. Zhou, L. Midolo, S. Scholz, A. D. Wieck, A. Ludwig, et al., *Science advances* **2020**, *6*, 50 eabc8268.

[163] A. Tiranov, V. Angelopoulou, C. J. van Diepen, B. Schrinski, O. A. D. Sandberg, Y. Wang, L. Midolo, S. Scholz, A. D. Wieck, A. Ludwig, et al., *Science* **2023**, *379*, 6630 389.

[164] Y. Arakawa, M. J. Holmes, *Applied Physics Reviews* **2020**, *7*, 2.

[165] D. Huber, M. Reindl, J. Aberl, A. Rastelli, R. Trotta, *Journal of Optics* **2018**, *20*, 7 073002.

[166] L. Zhai, M. C. Löbl, G. N. Nguyen, J. Ritzmann, A. Javadi, C. Spinnler, A. D. Wieck, A. Ludwig, R. J. Warburton, *Nature communications* **2020**, *11*, 1 4745.

[167] N. Tomm, A. Javadi, N. O. Antoniadis, D. Najer, M. C. Löbl, A. R. Korsch, R. Schott, S. R. Valentin, A. D. Wieck, A. Ludwig, et al., *Nature Nanotechnology* **2021**, *16*, 4 399.

[168] H. Wang, H. Hu, T.-H. Chung, J. Qin, X. Yang, J.-P. Li, R.-Z. Liu, H.-S. Zhong, Y.-M. He, X. Ding, et al., *Physical review letters* **2019**, *122*, 11 113602.

[169] D. Huber, M. Reindl, Y. Huo, H. Huang, J. S. Wildmann, O. G. Schmidt, A. Rastelli, R. Trotta, *Nature communications* **2017**, *8*, 1 15506.

[170] P. Lodahl, A. Floris van Driel, I. S. Nikolaev, A. Irman, K. Overgaag, D. Vanmaekelbergh, W. L. Vos, *Nature* **2004**, *430*, 7000 654.

[171] K. Hennessy, A. Badolato, M. Winger, D. Gerace, M. Atatüre, S. Gulde, S. Fält, E. L. Hu, A. Imamoğlu, *Nature* **2007**, *445*, 7130 896.

[172] Z. Luo, S. Sun, A. Karasahin, A. S. Bracker, S. G. Carter, M. K. Yakes, D. Gammon, E. Waks, *Nano letters* **2019**, *19*, 10 7072.

[173] A. G. Curto, G. Volpe, T. H. Taminiau, M. P. Kreuzer, R. Quidant, N. F. Van Hulst, *Science* **2010**, *329*, 5994 930.

[174] N. Livneh, M. G. Harats, D. Istrati, H. S. Eisenberg, R. Rapaport, *Nano letters* **2016**, *16*, 4 2527.

[175] M. Pfeiffer, K. Lindfors, H. Zhang, B. Fenk, F. Phillipp, P. Atkinson, A. Rastelli, O. G. Schmidt, H. Giessen, M. Lippitz, *Nano letters* **2014**, *14*, 1 197.

[176] J. Claudon, J. Bleuse, N. S. Malik, M. Bazin, P. Jaffrennou, N. Gregersen, C. Sauvan, P. Lalanne, J.-M. Gérard, *Nature Photonics* **2010**, *4*, 3 174.

[177] M. E. Reimer, G. Bulgarini, N. Akopian, M. Hocevar, M. B. Bavinck, M. A. Verheijen, E. P. Bakkers, L. P. Kouwenhoven, V. Zwiller, *Nature communications* **2012**, *3*, 1 737.

[178] N. Somaschi, V. Giesz, L. De Santis, J. Loredo, M. P. Almeida, G. Hornecker, S. L. Portalupi, T. Grange, C. Anton, J. Demory, et al., *Nature Photonics* **2016**, *10*, 5 340.

[179] A. Faraon, P. E. Barclay, C. Santori, K.-M. C. Fu, R. G. Beausoleil, *Nature Photonics* **2011**, *5*, 5 301.

[180] J. Liu, R. Su, Y. Wei, B. Yao, S. F. C. d. Silva, Y. Yu, J. Iles-Smith, K. Srinivasan, A. Rastelli, J. Li, et al., *Nature nanotechnology* **2019**, *14*, 6 586.

[181] K. Watanabe, N. Koguchi, Y. Gotoh, *Japanese Journal of Applied Physics* **2000**, *39*, 2A L79.

[182] M. Gurioli, Z. Wang, A. Rastelli, T. Kuroda, S. Sanguinetti, *Nature materials* **2019**, *18*, 8 799.

[183] S. F. C. da Silva, G. Undeutsch, B. Lehner, S. Manna, T. M. Krieger, M. Reindl, C. Schimpf, R. Trotta, A. Rastelli, *Applied Physics Letters* **2021**, *119*, 12.

[184] C. Schimpf, M. Reindl, F. Basso Basset, K. D. Jöns, R. Trotta, A. Rastelli, *Applied Physics Letters* **2021**, *118*, 10.

[185] S. Prescott, P. P. Iyer, S. Addamane, H. Jung, T. S. Luk, I. Brener, O. Mitrofanov, *Nanophotonics* **2024**, , 0.

[186] M. Khoury, H. Quard, T. Herzig, J. Meijer, S. Pezzagna, S. Cueff, M. Abbarchi, H. S. Nguyen, N. Chauvin, T. Wood, *Advanced Optical Materials* **2022**, *10*, 21 2201295.

[187] K. A. Sergeeva, D. V. Pavlov, A. A. Seredin, E. V. Mitsai, A. A. Sergeev, E. B. Modin, A. V. Sokolova, T. C. Lau, K. V. Baryshnikova, M. I. Petrov, S. V. Kershaw, A. A. Kuchmizhak, K. S. Wong, A. L. Rogach, *Advanced Functional Materials* **2023**, *33*, 44 2307660.

[188] P. P. Iyer, S. Prescott, S. Addamane, H. Jung, E. Renteria, J. Henshaw, A. Mounce, T. S. Luk, O. Mitrofanov, I. Brener, *Nano Letters* **2024**, *24*, 16 4749.

[189] X. Liu, Y. Kan, S. Kumar, D. Komisar, C. Zhao, S. I. Bozhevolnyi, *Science Advances* **2023**, *9*, 32 eadh0725.

[190] T.-Y. Huang, R. R. Grote, S. A. Mann, D. A. Hopper, A. L. Exarhos, G. G. Lopez, A. R. Klein, E. C. Garnett, L. C. Bassett, *Nature communications* **2019**, *10*, 1 2392.

[191] S. Liu, K. Srinivasan, J. Liu, *Laser & Photonics Reviews* **2021**, *15*, 10 2100223.

[192] W. Redjem, Y. Zhiyenbayev, W. Qarony, V. Ivanov, C. Papapanos, W. Liu, K. Jhuria, Z. Al Balushi, S. Dhuey, A. Schwartzberg, et al., *Nature communications* **2023**, *14*, 1 3321.

[193] A. Vaskin, R. Kolkowski, A. F. Koenderink, I. Staude, *Nanophotonics* **2019**, *8*, 7 1151.

[194] V. Rutckaia, F. Heyroth, A. Novikov, M. Shaleev, M. Petrov, J. Schilling, *Nano letters* **2017**, *17*, 11 6886.

[195] Y. Park, H. Kim, J.-Y. Lee, W. Ko, K. Bae, K.-S. Cho, *Nanophotonics* **2020**, *9*, 5 1023.

[196] J. Bohn, T. Bucher, K. E. Chong, A. Komar, D.-Y. Choi, D. N. Neshev, Y. S. Kivshar, T. Pertsch, I. Staude, *Nano letters* **2018**, *18*, 6 3461.

[197] Y. Bao, Q. Lin, R. Su, Z.-K. Zhou, J. Song, J. Li, X.-H. Wang, *Science advances* **2020**, *6*, 31 eaba8761.

[198] S. Prescott, P. P. Iyer, H. Jung, T. S. Luk, J. Henshaw, A. Mounce, S. J. Addamane, I. Brener, O. Mitrofanov, In *Metamaterials, Metadevices, and Metasystems 2023*. SPIE, **2023** PC1264615.

[199] L. A. T. Greif, S. T. Jagsch, M. R. Wagner, A. Schliwa, *ACS Photonics* **2018**, *5*, 12 4838.

[200] A. Mittelstädt, L. A. T. Greif, A. Schliwa, *Physical Review B* **2021**, *104*, 11 115309.

[201] M. Jeong, B. Ko, C. Jung, J. Kim, J. Jang, J. Mun, J. Lee, S. Yun, S. Kim, J. Rho, *Nano Letters* **2024**, *24*, 19 5783.

[202] T. Santiago-Cruz, A. Fedotova, V. Sultanov, M. A. Weissflog, D. Arslan, M. Younesi, T. Pertsch, I. Staude, F. Setzpfandt, M. Chekhova, *Nano Lett.* **2021**, *21*, 10 4423.

[203] T. Stav, A. Faerman, E. Maguid, D. Oren, V. Kleiner, E. Hasman, M. Segev, *Science* **2018**, *361*, 6407 1101.

[204] K. Wang, J. G. Titchener, S. S. Kruk, L. Xu, H.-P. Chung, M. Parry, I. I. Kravchenko, Y.-H. Chen, A. S. Solntsev, Y. S. Kivshar, D. N. Neshev, A. A. Sukhorukov, *Science* **2018**, *361*, 6407 1104.

[205] T. Santiago-Cruz, S. D. Gennaro, O. Mitrofanov, S. Addamane, J. Reno, I. Brener, M. V. Chekhova, *Science* **2022**, *377*, 6609 991.

[206] C. Son, V. Sultanov, T. Santiago-Cruz, A. P. Anthur, H. Zhang, R. Paniagua-Dominguez, L. Krivitsky, A. I. Kuznetsov, M. V. Chekhova, *Nanoscale* **2023**, *15* 2567.

[207] L. Li, Z. Liu, X. Ren, S. Wang, V.-C. Su, M.-K. Chen, C. H. Chu, H. Y. Kuo, B. Liu, W. Zang, G. Guo, L. Zhang, Z. Wang, S. Zhu, D. P. Tsai, *Science* **2020**, *368*, 6498 1487–1490.

[208] J. Zhang, J. Ma, M. Parry, M. Cai, R. Camacho-Morales, L. Xu, D. N. Neshev, A. A. Sukhorukov, *Science Advances* **2022**, *8*, 30 eabq4240.

[209] J. Ma, J. Zhang, Y. Jiang, T. Fan, M. Parry, D. N. Neshev, A. A. Sukhorukov, *Nano Letters* **2023**, *23*, 17 8091.

[210] M. A. Weissflog, J. Ma, J. Zhang, T. Fan, S. Lung, T. Pertsch, D. N. Neshev, S. Saravi, F. Setzpfandt, A. A. Sukhorukov, *Nanophotonics* **2024**.

[211] C. W. Hsu, B. Zhen, A. D. Stone, J. D. Joannopoulos, M. Soljačić, *Nat. Rev. Mater.* **2016**, *1*, 9.

[212] J. Noh, T. Santiago-Cruz, V. Sultanov, C. F. Doiron, S. D. Gennaro, M. V. Chekhova, I. Brener, Quantum pair generation in nonlinear metasurfaces with mixed and pure photon polarizations, **2024**, URL `https://arxiv.org/abs/2409.04569`.

[213] W. Jia, G. Saerens, Ü.-L. Talts, H. Weigand, R. J. Chapman, L. Li, R. Grange, Y. Yang, Polarization-entangled photon pair generation from an epsilon-near-zero metasurface, **2024**, URL `https://arxiv.org/abs/2405.03493`, ArXiv. 2405.03493.

[214] J. Ma, J. Ren, J. Zhang, J. Meng, C. McManus-Barrett, K. B. Crozier, A. A. Sukhorukov, *arXiv.org* **2024**, arXiv:2408.02903.

[215] Z. Liu, Y. Xu, Y. Lin, J. Xiang, T. Feng, Q. Cao, J. Li, S. Lan, J. Liu, *Phys. Rev. Lett.* **2019**, *123* 253901.

[216] J. Yang, P. Dichtl, J. Flórez, C. C. Phillips, A. S. Clark, R. F. Oulton, In G. S. Subramania, S. Foteinopoulou, editors, *Active Photonic Platforms 2022*, volume 12196. International Society for Optics and Photonics, SPIE, **2022** 121960E, URL `https://doi.org/10.1117/12.2633949`.

[217] S. Molesky, Z. Lin, A. Y. Piggott, W. Jin, J. Vucković, A. W. Rodriguez, *Nature Photonics* **2018**, *12*, 11 659.

[218] T. W. Hughes, M. Minkov, I. A. Williamson, S. Fan, *ACS Photonics* **2018**, *5*, 12 4781.

[219] S. Desai, S. Addamane, J. Y. Tsao, I. Brener, L. P. Swiler, R. Dingreville, P. P. Iyer, In *Proceedings of the AAAI Conference on Artificial Intelligence*, volume 39. **2025** 146–154.